TAMPERE UNIVERSITY OF TECHNOLOGY
Department of Science and Engineering

LASSE ORSILA

INTERFEROMETRIC DIELECTRIC REFLECTORS FOR DISPERSION COMPENSATION IN FIBRE LASERS

MASTER OF SCIENCE THESIS

The subject was approved by the department council on May 7th, 2003.

Examiners: Professor Oleg Okhotnikov
Ph.D. Mircea Guina

Preface

This work has been carried out at the Optoelectronics Research Centre of Tampere University of Technology.

First, I want to express my deepest gratitude to Professor Oleg Okhotnikov, who made this work, that first seemed insuperable, possible and for his constant belief that I can overcome all the problems I face during the work. And moreover I thank him for his wisdom to choose an attainable target for my thesis without compromising the work's significance. Secondly, I thank Mircea Guina for his guidance to scientific work and ways to face grave problems in research work.

I would like to thank my friends at ORC, especially Luis Gomes, for the help with fibre laser measurements, Antti Härkönen, for discussions about the work, Antti Isomäki, for the help with LaTeX and dispersion issues, Markus Peltola, for his long hours with the electron beam evaporator, Matei Rusu for cheering up the atmosphere and helping with all the little electronic gadgets in the lab. In addition, I give thanks to Markku Leino in physics institute for sharing his experience with LaTeX in fine tuning some of my intricate matrix equations. I also thank Liekki Oy for providing the Yb-doped fibre.

Last, I thank my parents for supporting my studies, my parents in law for optimism for my work and most important my beloved wife, Reetta, for her compassion and support during all these years.

Tampere, May 31th, 2003

Lasse Orsila

Contents

Abstract **v**

Tiivistelmä **vi**

Abbreviations and symbols **viii**

1 Introduction **1**

2 Theory **3**
2.1 Light-matter interaction . . . 3
2.2 Optical thin film reflectors . . . 5
2.2.1 High reflective coatings . . . 6
2.2.2 Anti-reflective coatings . . . 8
2.3 Dispersion . . . 10
2.3.1 Group delay and dispersion parameters . . . 11
2.3.2 Dispersion induced pulse broadening . . . 13
2.4 Conventional dispersion compensation methods . . . 15
2.4.1 Fibre methods for dispersion compensation . . . 15
2.4.2 Prism pair . . . 16
2.4.3 Grating pair . . . 18
2.4.4 Chirped mirrors . . . 18
2.4.5 Gires-Tournois interferometer . . . 20
2.5 Electron beam evaporation . . . 23

3 GTI fabrication and characterization **28**
3.1 Calibration . . . 28
3.1.1 Thickness calibration . . . 29
3.1.2 Refractive index measurement . . . 30
3.2 GTI design procedure . . . 31
3.3 Evaporation procedure . . . 32
3.4 Measurements of thin film mirrors . . . 34

3.5 Dispersion measurements 35

4 Results and conclusions **37**
4.1 Testing a GTI in a fibre laser cavity 37
4.2 Fibre laser performance with a GTI 38
4.3 Conclusions 40

5 Summary **42**

Bibliography **43**

A Operation instructions for EB-system **48**

Abstract

TAMPERE UNIVERSITY OF TECHNOLOGY
Department of Science and Engineering
Institute of Physics
Optoelectronics Research Centre
Orsila, Lasse: ”Interferometric Dielectric Reflectors for Dispersion Compensation in Fibre Lasers”
Master of Science Thesis, 54 pages
Examiners: Professor Oleg Okhotnikov and Ph.D. Mircea Guina
May 2003

This thesis deals with manufacturing dielectric Gires-Tournois interferometers by means of electron beam evaporation and exploiting them for dispersion compensation in a $\sim$1 μm mode-locked fibre laser cavity. Optical fibres have normal dispersion at this region and thereby our dispersive mirror should donate a higher negative dispersion in order to have average anomalous group-velocity dispersion.

Optical thin films can be designed to have sophisticated reflectivity spectra and dispersion properties. However, evaporation accuracy, absorbtion and adhesion limit the realisation of these films. Therefore we have tried to find a good balance between performance and processability, yet providing required dispersion.

This work had a practical, experimental way of approaching the problem and with the aid of numerical simulations, several trials, and errors, were made to achieve the target. As a result we obtained self-started 1.5 ps pulse mode-locked operation at 1022.8 nm with a repetition rate of 95 MHz. In terms of pulse width this corresponds to one order of magnitude improvement compared to the uncompensated situation.

Tiivistelmä

TAMPEREEEN TEKNILLINEN YLIOPISTO
Teknis-luonnontieteellinen osasto
Fysiikan laitos
Optoelektroniikan tutkimuskeskus
Orsila, Lasse: ”Interferometric Dielectric Reflectors for Dispersion Compensation in Fibre Lasers”
Diplomityö, 54 sivua
Tarkastajat: Professori Oleg Okhotnikov ja TkT Mircea Guina
Toukokuu 2003

Optisen tietoliikenteen kehitys on tuonut mukanaan uusia sovelluksia optoelektroniikan alalle. Eräs uudemmista sovelluksista on kuitulaserit, joissa valo kulkee edestakaisin ja vahvistuu optisesti viritetyssä erikoiskuidussa, jolloin kuitu toimii perinteisen laserin kaviteetin tapaan. Sovellettaessa kuitulasereita uusilla aallonpituuksilla ja uusissa sovelluksissa, kuitulasereiden tarvitsee toimia niille dispersion kannalta epäedullisemmilla aallonpituuksilla. Valon dispersio tarkoittaa, että eri valon taajuudet kulkevat eri nopeudella väliaineessa — eikä riippuvuus tällöin ole lineaarista. Yhden mikrometrin aallonpituudella kuitulaserissa tätä epäideaalisuutta tasapainottamaan tarvitaan dispersiota kompensoiva osio. Tämän johdosta tämän työn tavoitteena oli valmistaa elektronisuihkuhöyrystimellä dielektrisiä peilejä, jotka toimivat toisaalta kaviteetin päätypeilinä ja toisaalta kompensoivat optisen kuidun luontaisen dispersion.

Elektronisuihkuhöyrystys on tyhjiökammiossa suoritettava ohutkalvorakenteiden valmistusmenetelmä, jossa suurienergisiä elektroneja kiihdytetään höyrystettävän materiaalin pintaan. Muodostuva kaasuvuo kulkeutuu tyhjiökammion yläosassa olevan näytteen pinnalle ja muodostaa mikroskooppisen ohuita kerroksia. Klassisen aalto-optiikan perusteella ohuille, tasaisille kalvoille voidaan johtaa heijastuvuus ja dispersion ominaisuudet.

Tässä työssä keskeisimpänä aiheena oli Gires-Tournois-interferometrin (GTI) valmistaminen ja sen soveltaminen kuitulaserin kaviteetin dispersion kompensoimiseen. GTI:n toiminta dispersiivisenä peilinä perustuu ohutkalvorakenteen sisällä tapahtuvaan resonanssiin, jossa eri aallonpituudet kokevat eri mittaisen ryhmäviiveen. Kun ryhmäviiveen muutosno-

peus on positiivinen aallonpituuden funktiona, niin sanotaan, että kalvolla on epänormaali dispersio tällä aallonpituusalueella. Suuren epänormaalin dispersion omaava peili yhdistettynä normaalin dispersion omaavaan lyhyeen optiseen kuituun tuottaa keskimääräisesti pienen epänormaalin dispersion, joka on laserin toiminnan kannalta edullinen tilanne. Jos kuitulaserin kaviteettiin jää suuri dispersio, niin siinä kulkevat pulssit levenevät nopeasti luonnostaan.

Kuitulasereista halutaan saada lyhyitä pulsseja, jotta niitä voidaan soveltaa erinäisissä lääketieteellisissä sovelluksissa ja mittausjärjestelmissä. Lyhyiden pulssien merkitys korostuu lääketieteessä kun esimerkiksi halutaan leikata kudosta intensiivisillä valopulsseilla pitäen keskimääräinen teho pienenä, jotta kudos ja sen ympäristö ei kuumenisi. Mittaussovelluksissa lyhyitä pulsseja voidaan soveltaa tilanteissa, joissa mittaukseen käytettävä laser muutoin vaikuttaisi mitattavaan suureeseen, mutta pulssin kestäessä vain muutaman pikosekunnin mitään merkittävään muutosta kohteessa ei ehdi tapahtumaan. Lyhyitä pulsseja tarvitaan myös tietoliikennesovelluksissa, kun halutaan siirtää kuidussa tietoa nopeasti entistä tiheämmin peräkkäin kulkevilla pulsseilla. Mikäli pulssit ovat liian pitkiä on vaarana, että ne sekoittuvat keskenään estäen tiedonsiirron.

Tässä diplomityössä lähestyttiin tavoitteita kokeellisesta näkökulmasta: matemaattisia malleja ja laskelmia apuna käyttäen suoritettiin vuoden aikana joukko systemaattisia kokeita, joiden edetessä saatiin valmistettua halutun kaltaisia dispersiivisiä peilejä. Työn tavoitteet saavutettiin yli odotusten: käytettäessä elektronisuihkuhöyrystimellä valmistettua GTI:tä kuitulaserin kaviteetin toisena päätypeilinä laser toimi itsestään käynnistyvänä moodilukittuna laserina 1022,8 nm aallonpituudella. Laserin tuottamien pulssien kesto oli vain 1,5 ps toistotaajuuden ollessa 95 MHz. Kun GTI korvattiin tavallisella metallipeilillä sama laser toimi moodilukittuna, mutta pulssien kesto oli kymmenkertainen. Tämä osoittaa, että valmistetut peilit toimivat suunnitellulla tavalla.

Saatujen onnistuneiden tulosten perusteella on mahdollista, että tässä työssä käytetty kompensointimenetelmä syrjäyttäisi perinteisiä dispersiota kompensoivia menetelmiä. Kuten monessa muussakin tutkimuksessa, niin vasta pitkäjänteisen tuotekehityksen jälkeen laboratoriossa esitettyjä tuloksia voidaan soveltaa kaupallisessa tarkoituksessa. Ratkaistavina ongelmina on edelleen ainakin resonanssitaajuuden tarkka sijoittaminen ja prosessin toistettavuus.

Abbreviations and symbols

AFP	Asymmetric Fabry-Pérot
COD	Catastrophic Optical Damage
CDBR	Chirped Distributed Bragg Reflector
DBR	Distributed Bragg Reflector
DCF	Dispersion Compensating Fibre
DFF	Dispersion-Flattened Fibre
DND	Direct Nanoparticle Deposition
DSF	Dispersion-Shifted Fibre
Er	Erbium
FP	Fabry-Pérot
FWHM	Full-Width at Half Maximum
GaAs	Gallium-Arsenide
GDD	Group Delay Dispersion
GTI	Gires-Tournois Interferometer
GVD	Group-Velocity Dispersion
InGaAs	Indium-Gallium-Arsenide
InGaNAs	Indium-Gallium-Nitride-Arsenide
InP	Indium-Phosphide
MBE	Molecular Beam Epitaxy
NLS	Nonlinear Schrödinger Equation
SESAM	Semiconductor Saturable Absorber Mirror
SMF	Single-Mode Fibre
SPM	Self-Phase Modulation
TF	Tooling Factor

α	Absorption coefficient
β	Propagation constant
β_2	Group-velocity dispersion parameter
γ	Nonlinear parameter
γ_j	Damping coefficient describing losses in material
δ	Round-trip phase change
φ	Phase change on the GTI back mirror
λ	Wavelength
τ	Group delay time
ω	Optical frequency
ω_{0j}	Characteristic frequency at which an atom may absorb or emit radiant energy
Φ	Resultant phase change
ϕ''	Group delay dispersion
Ψ	Ellipsometric parameter
$\overline{a}$	Acceleration vector
$\overline{B}$	Magnetic field vector
c	Speed of light in vacuum
d	Cavity length or layer thickness or beam diameter
D	Dispersion parameter
D_l	Refraction matrix for normal incidence in layer l
D_p	Refraction matrix for p-polarization
D_s	Refraction matrix for s-polarization
e	Electron charge
f_j	Weighting factor known as oscillator strength or transition propability
$\overline{F}$	Lorentz force
I	Intensity of light
L	Propagation length
$\overline{k}$	Wave vector
m_e	The electron mass
n	Refractive index
N	Contributing electrons per unit volume
N_q	Frequency constant for quartz crystal
P	Path distance
P_0	Pulse peak power
q_e	Electron charge

R	Reflectivity of a thin film structure
r	Reflectance
$\bar{v}$	Velocity vector
v_g	Group-velocity
Z	Accoustic impedance

Chapter 1

Introduction

The generation of ultrashort optical pulses continues to be a very active field of research. This technology has found application in areas of biomedical optics, high-speed communications and the fundamental study of ultrafast nonlinear processes in various materials and systems. Using laser pulses of a few tens of femtoseconds, chemists can study the motion of atoms during chemical reactions and biologists can witness the earliest steps in the natural processes, such as photosynthesis. Moreover owing to their broad spectra short optical pulses represent important tools in medical imaging techniques.

In the past decades, diode pumped solid-state lasers have dominated area of tunable ultrashort pulse light sources offering not only extremely short optical pulses comprising several optical cycles but also broad tunability. Recent unprecedented growth of the telecom industry had resulted in the development of a mature fibre technology and reliable and cost effective components, which makes suitably designed fibre lasers real contenders to conventional solid state lasers. The broad fluorescence spectrum makes different fibre gain media attractive for tunable and ultrashort pulse sources. Continues wave operation for a Nd:glass fibre laser has been reported over a tuning range of 30 nm FWHM and more recently over 50 nm FWHM. For Er-doped fibre lasers, tuning over 35 nm has been achieved in an actively mode-locked system and over 50 nm in an additive-pulse mode-locked fibre soliton laser. For fibre lasers doped with thulium, which exhibits a particularly wide fluorescence spectrum, a tuning range as wide as 100 nm has been demonstrated.

Ytterbium-doped silica fibre having a broad gain bandwidth, a high optical conversion

efficiency, and a large saturation fluence offers almost ideal gain medium for the generation and the amplification of wavelength-tunable ultrashort optical pulses. Ytterbium-doped fibre-lasers and fibre-amplifiers can operate in the spectral region from 970 to 1150 nm. In this broad wavelength range there is a number of applications ranging from micro-machining at fundamental wavelengths to bio-medical applications at frequency-doubled wavelengths. Despite significant attention to development of practical, user-friendly mode-locked source operating in the region of 1 μm, there are very few reports on successful demonstration of passively mode-locked lasers and there are no reports on tunable fibre-based picosecond sources. Additional interesting feature of the Yb-doped fibre lasers is that under certain conditions those lasers can operate in the 977 nm spectral band, which make them very attractive as a master source for frequency doubling to achieve 488 nm and thus to substitute bulky and inefficient Ar-ion lasers.

The generation of sub-picosecond pulses by means of mode-locked lasers usually requires operation in the regime of negative group delay dispersion of the laser cavity. The main difficulty associated with pulse generation within ytterbium-doped fibres results from the high value of normal material dispersion for silica at wavelengths below 1.1 μm. Although waveguide dispersion has been used generally to balance the material dispersion at longer wavelength (>1.3 μm), it does not appear feasible to achieve overall anomalous dispersion by this approach for such a short wavelength. By use of bulk dispersion compensating elements within the cavity the average dispersion can be either normal or anomalous and thus stretched-pulse or soliton pulse regimes have been obtained. However, bulk dispersion compensators are not easily integrated within fibre lasers and lead to additional drawbacks such as increased size of the system.

The purpose of this thesis was to investigate better techniques to control the dispersion properties of mode-locked fibre lasers. More concrete, the thesis is concerned with advanced dielectric reflectors in a form of Gires-Tournois interferometers (GTIs). Next sections provide a detailed description of the design, fabrication technology and application of GTIs for dispersion compensation of Yb-doped mode-locked fibre lasers.

Chapter 2

Theory

This chapter concerns theoretical issues meant to explain the optical properties of dielectric thin films. The analysis is focused on dielectric dispersive mirrors and their reflectivity and dispersion properties.

2.1 Light-matter interaction

Light is a basic element of our life and we all have a clear image about it. However, in order to fully understand its properties we have to make use of theoretical formalism such as wave optics. The equation describing the propagation of a light beam consisting of discrete frequency components ω_i is given by [Hec98]:

$$\Psi(z,t) = \sum_i A_i e^{i[\omega_i t - n(\omega_i)\bar{k}\cdot\bar{r}]}. \tag{2.1}$$

Here $\bar{k}$ represents the wave vector describing the propagation direction, $\bar{r}$ is the coordinate vector, $n(\omega_i)$ is the refractive index corresponding to frequency ω_i, and A_i is the amplitude of the frequency component ω_i. In simple terms, the optical wave equation is described by the phase term $\phi_i = \omega_i t - n(\omega_i)\bar{k}\cdot\bar{r}$ and amplitudes A_i.

In order to harness the modern mathematics to our disposal we need to consider a general case, where the optical wave has two components that propagate forward and backward, respectively. Thus we can write the wave equation as

$$\Psi = Ae^{i\phi} + Be^{-i\phi}, \tag{2.2}$$

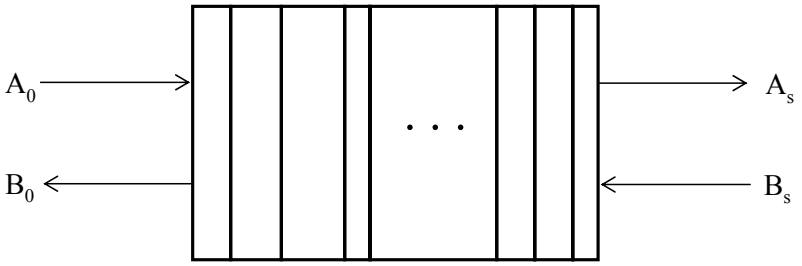

Figure 2.1: A schematic representation of a transfer matrix system.

where A and B are the amplitudes for the forward and backwards propagating components, respectively. For reasons which will become clear in the next paragraph, equation (2.2) is usually written in a matrix form as:

$$Ae^{i\phi} + Be^{-i\phi} \mapsto \begin{pmatrix} e^{i\phi} & 0 \\ 0 & e^{-i\phi} \end{pmatrix} \begin{pmatrix} A \\ B \end{pmatrix}. \tag{2.3}$$

This formulation is then used as a basis for the transfer matrix formalism [Yeh88] that is used to calculate the transmission and reflection of a multilayered optical systems. Figure 2.1 shows a schematic representation of such a system, where $\binom{A_0}{B_0}$ and $\binom{A_s}{B_s}$ represent the forward and backwards propagating components at the interface with the first and the last layer, respectively. The system consists of N individual layers with parallel interfaces.

Generally speaking, the relation between the optical field at the input and at the output of a multilayered system is given by

$$\begin{pmatrix} A_0 \\ B_0 \end{pmatrix} = \begin{pmatrix} M_{11} & M_{12} \\ M_{21} & M_{22} \end{pmatrix} \begin{pmatrix} A_s \\ B_s \end{pmatrix}. \tag{2.4}$$

In order to make use of this formalism we should understand how the terms of the transfer matrix are related to the physical properties of the system. First of all, the light propagating in a layer l is described by the propagation matrix

$$P_l = \begin{pmatrix} e^{i\phi_l} & 0 \\ 0 & e^{-i\phi_l} \end{pmatrix}, \tag{2.5}$$

where ϕ_l is the phase shift given as

$$\phi_l = k_l d_l = \frac{2\pi n_l(\lambda)}{\lambda} d_l. \tag{2.6}$$

Here k_l is the propagation constant, d_l is the layer thickness and $n_l(\lambda)$ is the refractive index. We should note that in a general case n_l is wavelength dependent and contains an imaginary term that accounts for absorption.

Other physical effects that play a role in calculating the transfer matrix are the reflection and refraction at the interface between adjacent layers. This can be described with a classical Snell's law:

$$n_a sin(\theta_a) = n_b sin(\theta_b), \tag{2.7}$$

where $n_{a,b}$ are refractive indices for materials a and b, respectively, and $\theta_{a,b}$ are the incident angle and refraction angle. In a more elaborate form the refraction and reflection at boundaries are accounted for by the boundary matrices D_l [Yeh88]. For transverse electric (TE) waves, or s-polarization,

$$D_{l,s} = \begin{pmatrix} 1 & 1 \\ n_l \cos\theta_l & -n_l \cos\theta_l \end{pmatrix} \tag{2.8}$$

and for p-polarization i.e. TM-polarization (Transverse Magnetic)

$$D_{l,p} = \begin{pmatrix} \cos\theta_l & \cos\theta_l \\ n_l & -n_l \end{pmatrix}. \tag{2.9}$$

In this thesis we are mainly interested in optical thin films examined from normal incidence or very small angle, θ. Therefore $\cos\theta \approx 1$ and hence $D_{l,s} \approx D_{l,p}$. Once matrices P_l and D_l are calculated for all layers, the transfer matrix of the system is given by

$$\begin{pmatrix} M_{11} & M_{12} \\ M_{21} & M_{22} \end{pmatrix} = D_0^{-1} \left[\prod_{l=1}^{N} D_l P_l D_l^{-1} \right] D_s. \tag{2.10}$$

This formalism can also be applied for layers with graded refractive index profile by splitting the individual layers in thin slices with constant refractive index. It should be noted that this model does not give accurate results for layers with thickness smaller than few nanometers. In those cases more complex formalism, based on quantum optics, has to be considered.

2.2 Optical thin film reflectors

A thin film is a layer or a stack of layers with certain refractive indices and absorption coefficients. Usually 20 μm is considered the upper limit for the thickness of a thin film. In our

case we assume that films are flat and all boundaries are parallel to each other. Phenomena like surface roughness and impurities are considered insignificant for its properties.

With the matrix notation from (2.4) it is easy to derive an expression for the reflectivity of a thin film. The reflectance r is give by

$$r = \frac{B_0}{A_0} \tag{2.11}$$

with $B_s = 0$. Equation (2.4) can now be written as

$$\begin{pmatrix} A_0 \\ B_0 \end{pmatrix} = \begin{pmatrix} M_{11}A_s \\ M_{21}A_s \end{pmatrix}. \tag{2.12}$$

The thin film reflectivity is the absolute value squared of the reflectance:

$$R = |r|^2 = \left|\frac{B_0}{A_0}\right|^2 = \left|\frac{M_{21}A_s}{M_{11}A_s}\right|^2 = \left|\frac{M_{21}}{M_{11}}\right|^2. \tag{2.13}$$

All components of M are functions of wavelength and they depend on refractive index n. An important property of materials used for manufacturing thin film is to be lossless and hence to have real refractive index.

This formalism has the disadvantage that analytical calculations become easily tedious. However, this algorithm can be easily implemented using any software that has linear algebra tools. The formalism becomes more complex in case of short pulse propagation due to effect of nonlinearities and higher order dispersion terms [CBJS86].

Optical coatings are thin films on a target surface. They have one or more layers of materials that have characteristic optical properties. Materials and layer thicknesses are designed based on required optical properties. Coatings that have a very high reflectivity over certain wavelength range are called high reflective (HR). Those having high transmission are called anti-reflective (AR) coatings.

2.2.1 High reflective coatings

A straightforward way of achieving high reflective mirrors is to coat a flat, smooth substrate with pure silver (Ag) or gold (Au). For silver this will give higher that 99% reflectivity over a broad spectrum from 900 nm to 10 μm. Gold coatings show even higher reflectivity

from about 0.9 μm to far infrared [Sav92]. Besides their simplicity, metallic coatings will absorb part of the incident radiation leading to signal loss. Optical absorption at high powers can lead to catastrophic optical damage (COD), usually originating from a defect inside the mirror. Metals have tendency to oxidise and they are usually protected with a thin dielectric layer. On the contrary dielectric HR mirrors are ideally lossless and therefore can achieve higher reflectivities and higher incident power.

Typical type of dielectric reflector is the distributed Bragg reflector (DBR). It consists of a substrate with a refractive index n_s followed by multiple pairs (N) of alternating low (n_L) and high (n_H) refractive index layers, each with an optical thickness (d) of target centre wavelength (λ_0) over four:

$$d = \frac{\lambda_0}{4n(\lambda)}. \tag{2.14}$$

λ_0 is also called the Bragg wavelength. When this structure is written in a transfer matrix form (eq. (2.5), (2.8) and (2.10)), we obtain:

$$P_l = \begin{pmatrix} e^{i\phi_l} & 0 \\ 0 & e^{-i\phi_l} \end{pmatrix} = \begin{pmatrix} i & 0 \\ 0 & -i \end{pmatrix} \tag{2.15}$$

and

$$D_l P_l D_l^{-1} = \begin{pmatrix} 1 & 1 \\ n_l & -n_l \end{pmatrix} \begin{pmatrix} i & 0 \\ 0 & -i \end{pmatrix} \frac{1}{2} \begin{pmatrix} 1 & \frac{1}{n_l} \\ 1 & -\frac{1}{n_l} \end{pmatrix} = i \begin{pmatrix} 0 & \frac{1}{n_l} \\ n_l & 0 \end{pmatrix}. \tag{2.16}$$

Furthermore, the DBR's transfer matrix is

$$\begin{aligned} M &= D_0^{-1} \left[\prod^N D_H P_H D_H^{-1} D_L P_L D_L^{-1} \right] D_s \\ &= \frac{(-1)^N}{2} \begin{pmatrix} 1 & \frac{1}{n_0} \\ 1 & -\frac{1}{n_0} \end{pmatrix} \left[\prod^N \begin{pmatrix} 0 & \frac{1}{n_H} \\ n_H & 0 \end{pmatrix} \begin{pmatrix} 0 & \frac{1}{n_L} \\ n_L & 0 \end{pmatrix} \right] \begin{pmatrix} 1 & 1 \\ n_s & -n_s \end{pmatrix} \\ &= \frac{1}{2}(-1)^N \begin{pmatrix} \left(\frac{n_L}{n_H}\right)^N + \frac{n_s}{n_0}\left(\frac{n_H}{n_L}\right)^N & \left(\frac{n_L}{n_H}\right)^N - \frac{n_s}{n_0}\left(\frac{n_H}{n_L}\right)^N \\ \left(\frac{n_L}{n_H}\right)^N - \frac{n_s}{n_0}\left(\frac{n_H}{n_L}\right)^N & \left(\frac{n_L}{n_H}\right)^N + \frac{n_s}{n_0}\left(\frac{n_H}{n_L}\right)^N \end{pmatrix}. \end{aligned} \tag{2.17}$$

This can then be substituted into equation (2.13) to get the formula of DBR reflectivity at λ_0:

$$R = \left|\frac{M_{21}}{M_{11}}\right|^2 = \left|\frac{\frac{n_s}{n_0} - \left(\frac{n_L}{n_H}\right)^{2N}}{\frac{n_s}{n_0} + \left(\frac{n_L}{n_H}\right)^{2N}}\right|^2 . \tag{2.18}$$

This result can be found in other equivalent forms ([Saa02], [Yeh88]). Nonetheless, it is important to realise that a reflectivity of 1 can never be reached. Using typical dielectric material materials, mirrors that reflect at least 99.999 % have been reliably demonstrated. With current technology the ultimate limiting factors for mirror reflectivity at a certain wavelength are the material losses [BC92] and DBR stack adhesion (too thick layer structures are not stable enough). A typical reflectivity curve is presented in the Figure 3.4. The DBR has a certain width $\Delta\lambda$, where it acts as a high reflective mirror. This width increases with increasing the difference between refractive indices of the DBR's layers, $\Delta n = n_H - n_L$, increases.

Typical dielectric materials for DBRs are TiO_2 (n=1.9-2.6), Ti_3O_5, TiO, Al_2O_3 (n=1.59) and SiO_2 (n=1.46). AlAs (n$\approx$ 2.9 at 1.5 μm), GaAs (n=3.5 at 1 μm) and other compound semiconductors can also be used. However, semiconductors have low losses only for certain wavelengths. In normal bulk optics, especially in visible range, MgF_2 (n=1.37 at 1 μm) is a very popular material because of its exceptionally low refractive index and low absorption coefficient.

Dielectric materials do not have the highest refractive index differences or always the right absolute value for the coating but they are usually chosen because they are lossless and have relatively constant refractive index over a broad wavelength range.

2.2.2 Anti-reflective coatings

Anti-reflective (AR) coatings are required to reduce surface reflectivity on some particular incident angle or over a broad incident angle. Broad angle AR coatings are used for example for eye glasses. Theoretically, AR coatings with zero reflectivity can be attained by using multiple lossless dielectric layers. In the following we describe common types of AR coatings based on their complexity:

- one λ/(4n) layer with $n_0 < n < n_s$, where n_0 is the refractive index of propagation

media, n the coating refractive index, and n_s the substrate refractive index.

- A particular case for the previous one: a very low reflectivity occurs when $n = \sqrt{n_0 n_s}$. Usually it is difficult to find a material to match this condition but in some common cases, such as air to glass interfaces, reflection can be reduced below 1% over a broad wavelength range with MgF_2 coating.

- three λ/(4n) layers with $n_0 < n_1 < n_2 < n_3 < n_s$ gives already a quite robust and low reflectance.

- $n_s|n_H|n_L|n_H|n_L|n_s$, where n_H and n_L are the high and low refractive index material, respectively, each with an optical thickness of about a quarter of the target wavelength. Elaborate calculations can be made to find a structure that gives a broad low reflectance spectrum in target area. Transmission bandwidth is usually limited rather to manufacturing accuracy than design issues.

- graded index refractive index profile i.e. $n = n(\lambda, d)$, where d is the depth from the surface, offer the best performance. Different kind of paraboloid or exponential refractive index profiles can give very broad transmission bands. These coatings are still more theoretical than practical solution because refractive index gradients are difficult to control during fabrication.

Reflectivity spectrum of a typical AR coating is presented in the Figure 2.2. In this example the coating consists of two pairs of SiO_2/TiO_2 layers. The structure is designed with a Matlab based computer program that implements the algorithm described in [Jea98].

AR coatings are to some extent more difficult to fabricate that coatings. The optimal solution is a compromise between the absolute value of the reflectivity, transmission bandwidth and robustness of the structure. Limiting factors are available materials and their refractive indices, absorption coefficients and the accuracy of controlling the thickness of each film during the deposition.

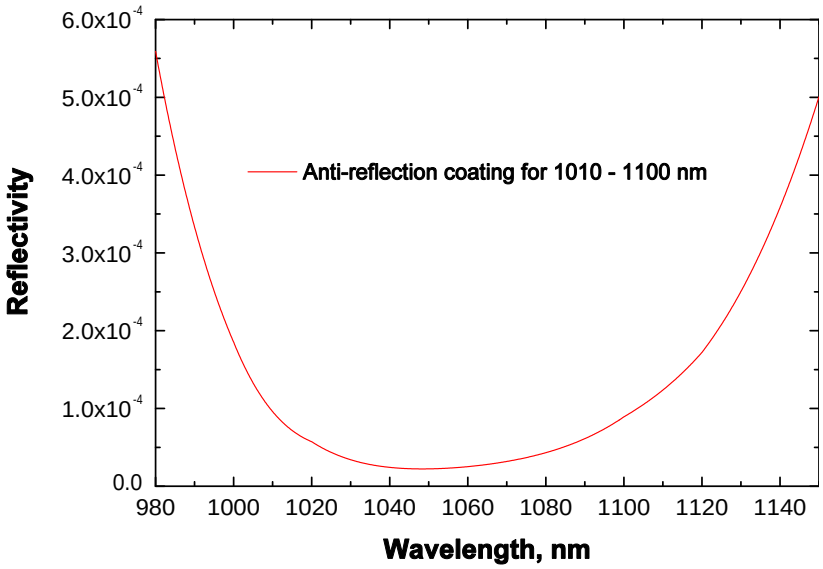

Figure 2.2: An example of an AR coating that is highly transparent in 1.01 μm–1.1 μm. The coating consists of 181.49/138/58.29/42.62 nm of SiO_2/TiO_2/SiO_2/TiO_2. GaAs was used as a substrate.

2.3 Dispersion

In this section I will explain the terminology and basic formula related to optical dispersion and its influence on the propagation of optical pulses. Generally speaking, the dispersion is the name given to any effect that cause different components of an optical signal to acquire a different delay when the signal is propagating over a fixed distance. In practice there are various mechanisms that introduce different types of dispersion. However, the most important one is the chromatic dispersion.

Chromatic dispersion is caused by the fact that different spectral components travel at different velocities. In optical fibres chromatic dispersion arises from two reasons: the wavelength dependence of the refractive index that leads to material dispersion and the radial power distribution of different optical frequencies that leads to waveguide dispersion.

For most materials the frequency dependence of refractive index is given by dispersion equation [Hec98]:

$$\frac{n(\omega)^2-1}{n(\omega)^2+2}=\frac{Nq_e^2}{3\varepsilon_0 m_e}\sum_j \frac{f_j}{\omega_{0j}^2-\omega^2+i\gamma_j\omega}, \tag{2.19}$$

where N is the amount of contributing electrons per unit volume, q_e is the electron charge, m_e is the electron mass, ω_{0j} are the characteristic frequencies at which an atom may absorb or emit radiant energy, f_j are weighting factors known as oscillator strengths or transition probabilities ($\sum_j f_j = 1$), and γ_j are the damping coefficients describing the losses in material.

Another way of finding the wavelength dependence of the refractive index is to know its absorption spectrum $\alpha(\omega)$ over a wide range and use Kramers-Krönig relation [Sin98]:

$$n(\omega) = n_0 + \frac{c}{\pi} P \int_0^\infty \frac{\alpha(\omega')}{\omega'^2 - \omega^2} d\omega', \tag{2.20}$$

where P stands for Cauchy principle value.

2.3.1 Group delay and dispersion parameters

Mathematically, chromatic dispersion can be quantified by means of different figure of merits, such as group-velocity dispersion (GVD), group delay dispersion (GDD) and dispersion parameter (D). To understand these figure of merits we recall again that chromatic dispersion arises because the refractive index depends on the optical frequency. Therefore, the propagation constant $\beta = n(\omega) \cdot k_0 = n(\omega) \cdot \frac{\omega}{c}$ does not depend linearly on ω, i.e. $\frac{d\beta}{d\omega} \neq$constant. $\frac{d\beta}{d\omega}$ is usually denoted by β_1 and β_1^{-1} represents the group-velocity, v_g.

$$v_g = \frac{c_0}{n_g} = \left(\frac{d\beta}{d\omega}\right)^{-1}, \tag{2.21}$$

where n_g is the group index [Nie02] given by

$$n_g = n + \omega \frac{dn}{d\omega} = n - \lambda \frac{dn}{d\lambda}. \tag{2.22}$$

The group-velocity tells how fast the envelope of an optical pulse propagates in a dispersive media. However, this does not tell how well the different spectral components of the pulse stay in the original phase relation. To understand the effect of dispersion on pulse propagation in an optical fibre we can assume that each spectral component travels independently and undergoes its own group delay, τ_g. Group delay describes the dispersive time delay induced by the spectral components of the pulse on length L. The group delay is

defined as

$$\tau_g = \frac{L}{v_g} = -\frac{d\phi}{d\omega} = \phi'. \tag{2.23}$$

If we consider two separate spectral components, ω_1 and $\omega_2; (\omega_2 > \omega_1)$, they propagate at a slightly different group velocities, v_{g_1} and v_{g_2}. As a result, while propagating in an optical media, they become separated in time by a delay

$$\Delta\tau = \frac{L}{v_{g_2}} - \frac{L}{v_{g_1}} = \phi_2' - \phi_1' \cong \phi'' \cdot (\omega_2 - \omega_1), \tag{2.24}$$

where $\phi'' = \frac{d^2\phi}{d\omega^2}$ is a quantity called the group delay dispersion (GDD) [Sve98].

There are several different ways to measure group delay ([Nie02], [BWK91]) and this information can then be used to determine group delay dispersion. By using $\omega = 2\pi c/\lambda$ and $d\omega = (-2\pi c/\lambda^2)\, d\lambda$ we get

$$\Delta\tau = \frac{d}{d\lambda}\left(\frac{L}{v_g}\right) d\lambda = D\, L\, d\lambda, \tag{2.25}$$

where D is the dispersion parameter defined as

$$D = \frac{d\tau_g}{d\lambda} = \frac{d}{d\lambda}\left(\frac{1}{v_g}\right) = -\frac{2\pi}{\lambda^2}\,\beta_2, \tag{2.26}$$

where β_2 is the group-velocity dispersion (GVD) parameter, $\beta_2 = \frac{d^2\beta}{d\omega^2}$. Group-velocity dispersion is a quantity connected particulary to optical fibres. It is calculated as

$$GVD = \beta_2 = \frac{d(1/v_g)}{d\omega} = \frac{\phi''}{L}. \tag{2.27}$$

It should be noted that GVD concept is well defined only for a homogeneous medium, like optical fibre. For an inhomogeneous media or a thin film structure, group delay dispersion is more a meaningful concept to consider. It gives the actual value of the total dispersion the entire system induces at a specific wavelength.

When we examine the pulse propagation [Agr01] and we are interested in the higher order dispersions, the dispersion can be taken into account by expanding the β into a Taylor series about the frequency ω_0 at which the pulse spectrum is centered:

$$\beta = n(\omega)\frac{\omega}{c} = \beta_0 + \beta_1(\omega - \omega_0) + \frac{1}{2}\beta_2(\omega - \omega_0)^2 + \cdots, \tag{2.28}$$

where

$$\beta_m = \left(\frac{d^m\beta}{d\omega^m}\right)_{\omega=\omega_0} \qquad (m = 0,1,2,\ldots). \tag{2.29}$$

The effect of the higher order dispersion terms $(\beta_3, \beta_4, \ldots)$ is often insignificant for the pulse broadening compared to the β_2. However, when pulse width is only few tens of femtoseconds, at least β_3 should be taken into account.

To link dispersion to material properties, we write a refractive index dependent expression for β_2:

$$\beta_2 = \frac{1}{c}\left(2\frac{dn}{d\omega} + \omega\frac{d^2n}{d\omega^2}\right). \tag{2.30}$$

When β_2 is positive we say that the system has normal dispersion and when β_2 is negative, then the system has anomalous dispersion. The wavelength where the sign changes is called the zero-dispersion wavelength, λ_D.

2.3.2 Dispersion induced pulse broadening

The propagation of the optical pulses in a dispersive media is mathematically treated with the Nonlinear Schrödinger equation (NLS). Nonlinear Schrödinger equation can be written in a form:

$$\frac{\partial A}{\partial z} + \frac{\alpha}{2}A + \frac{i\beta_2}{2}\frac{\partial^2 A}{\partial T^2} - \frac{\beta_3}{6}\frac{\partial^3 A}{\partial T^3} = i\gamma\left(|A|^2 A + \frac{i}{\omega_0}\frac{\partial}{\partial T}(|A|^2 A) - T_R A\frac{\partial |A|^2}{\partial T}\right), \tag{2.31}$$

where A is the slowly varying pulse envelope, α is the absorption coefficient, γ is the nonlinear coefficient, ω_0 is the carrier frequency, T_R is a parameter that describes delayed Raman response and appears as a self-frequency shift and

$$T = t - \frac{z}{v_g} \equiv t - \beta_1 z. \tag{2.32}$$

The equation (2.31) itself is difficult to harness for practical use. However, it can be simplified with few reasonable approximations. We consider a situation with low power ($\gamma \approx 0$) and negligible third order dispersion ($\beta_3 \approx 0$). With a new notation for normalized pulse amplitude U,

$$A(z,t) = \sqrt{P_0}\ \exp(-\alpha z/2)\, U(z,\tau), \tag{2.33}$$

where τ normalizes the time scale to the input pulse width T_0 ($1/e$ intensity),

$$\tau = \frac{T}{T_0} = \frac{t - z/v_g}{T_0} \tag{2.34}$$

and P_0 is the peak power of the pulse, we get a simplified form for the Schrödinger equation:

$$i\frac{\partial U}{\partial z} = \frac{\beta_2}{2}\frac{\partial^2 U}{\partial T^2}. \tag{2.35}$$

Equation (2.35) has a general solution

$$U(z,t) = \frac{1}{2\pi}\int_{-\infty}^{\infty}\int_{-\infty}^{\infty} U(0,T)\exp(i\omega T)dT\ \exp\left(\frac{i}{2}\beta_2\omega^2 z - i\omega T\right)d\omega \tag{2.36}$$

and it can have an arbitrary pulse shape. The effect of the dispersion can be analytically calculated for gaussian and hyperbolic secant pulses. A gaussian pulse is of the form

$$U(0,T) = \exp\left(-\frac{T^2}{2T_0^2}\right). \tag{2.37}$$

However, is it common to use full width at half maximum (FWHM) instead of T_0:

$$T_{FWHM} = 2\sqrt{(ln2)}T_0 \approx 1.6651092T_0. \tag{2.38}$$

The solution for the shape of a gaussian pulse at given location z can be obtained by substituting (2.37) into (2.36):

$$U(z,T) = \frac{T_0}{\sqrt{T_0^2 - i\beta_2 z}}\exp\left(-\frac{T^2}{2(T_0^2 - i\beta_2 z)}\right). \tag{2.39}$$

As it can be observed, a gaussian pulse maintains its shape but losses its amplitude and broadens during the propagation. Pulse width at position z [Agr97] can be expressed as

$$T(z) = T_0\sqrt{1 + \frac{|\beta_2|^2 z^2}{T_0^4}}. \tag{2.40}$$

From equation (2.40) we can see that the shorter the pulse the more significant the broadening effect is. This is why the dispersion compensation becomes critical even at short distances when pulses are sub-ps order. It should also be noted that the pulse width remains constant if $\beta_2 = 0$.

Hyperbolic secant pulses are visually close to gaussian pulses but their form

$$U(0,T) = sech\left(\frac{T}{T_0}\right)\exp\left(-\frac{iCT^2}{2T_0^2}\right) = \frac{2}{e^{\left(\frac{T}{T_0}\right)^2}+e^{\left(-\frac{T}{T_0}\right)^2}}\exp\left(-\frac{iCT^2}{2T_0^2}\right) \tag{2.41}$$

differs from gaussian in a important way. The C is the chirp parameter. Hyperbolic secant is the form of optical solitons.

2.4 Conventional dispersion compensation methods

It was shown before that the dispersion broadens the optical pulses. Compensating the dispersion can be done in various ways. In this section I will describe the most important conventional dispersion compensation methods and in addition Gires-Tournois Interferometer. Compensating methods can be divided into two main categories: fibre and free space based. At this point it is important to remember that we are mainly discussing how to compensate GDD, which is the average GVD times cavity length L. This leaves higher order dispersions uncompensated. Nonetheless, they are usually much smaller and can be considered insignificant. Provided that sub-10-fs pulses are needed, compensating third order dispersion is without doubt needed [WMG+02].

2.4.1 Fibre methods for dispersion compensation

Optical fibres are divided into different types (see Figure 2.3) according to their dispersion properties. Fibre dispersion properties are determined by their material and waveguide dispersion. Material dispersion can be slightly changed by adjusting the fibre composition. Whereas waveguide dispersion is determined by the fibre core-cladding geometry.

Dispersion shifted fibres (DSF) behave like standard fibres but their zero dispersion wavelength is shifted to 1550 nm. Dispersion flattened fibres (DFF) are special fibres that have a low and very constant dispersion over a broad wavelength range. Dispersion compensating fibres (DCF) have the opposite slope in the dispersion wavelength curve than the standard fibre. Dispersion compensation using optical fibers is very convenient to implement. However, requires rather long fibres and can introduce significant nonlinear effect

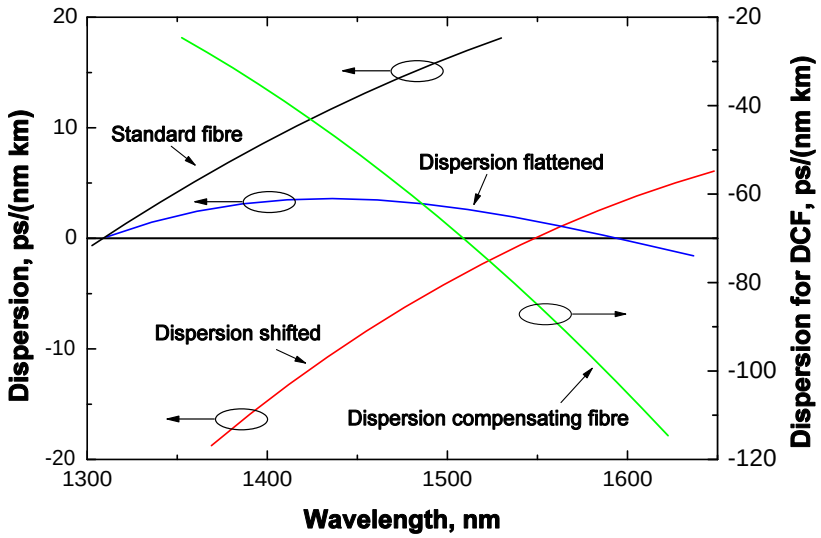

Figure 2.3: Dispersion curves for typical standard, dispersion shifted,dispersion flattened and dispersion compensating fibres (for DCF from [THF+99]).

that can limit their application. It is very important to note that at 1 μm wavelength, standard optical fibres have only normal dispersion. This is a considerable drawback for building mode-locked fibre lasers operating in the wavelength range around 1 μm.

2.4.2 Prism pair

A prism sequence, shown in the Figure 2.4, is a classical solution for creating negative or positive dispersion in a laser cavity [Sve98], [FMG84]. Prisms are generally used at minimum deviation angle, i.e. with incident angle equal to the exiting angle. The apex angle, ϕ, should be cut in such a way that rays enter and leave each prism at Brewster's angle. This minimizes reflection losses from prism surfaces.

The negative dispersion occurs when shorter wavelengths have smaller delay, i.e. $\Delta\tau_g < 0$, where $\Delta\tau_g = \tau_g(\omega_1) - \tau_g(\omega_2), \omega_1 > \omega_2$. Yet, in this configuration the phase delay for the blue components is larger than that for the red components since $\frac{dP}{d\lambda}$, where P is the path distance, is negative. The group-velocity, however, is determined by $\frac{d^2P}{d^2\lambda}$. Thus the blue components traverse the prism sequence in a shorter time than do the red components,

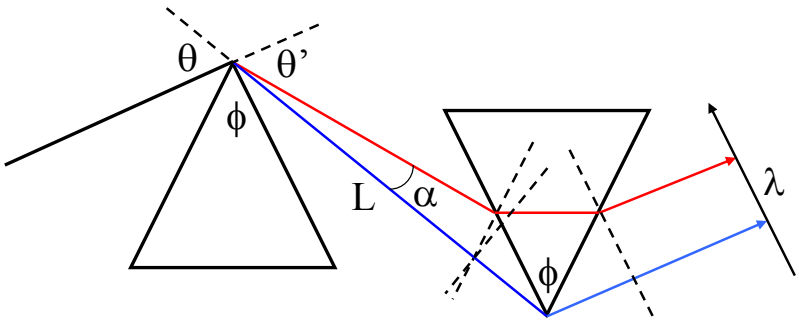

Figure 2.4: A prism pair inducing negative group delay dispersion.

despite the negative value of $\frac{dP}{d\lambda}$. This phenomena is illustrated in the Figure 2.5. Detailed calculations are presented in [FMG84] and [Zha02]. The GVD due to angular dispersion is

$$\Psi''_{\alpha}(\lambda_0) = \left.\frac{d^2\Psi}{d\omega^2}\right|_{\lambda_0} = -4L\frac{\lambda_0^3}{2\pi c^2}\left(\left.\frac{dn}{d\lambda}\right|_{\lambda_0}\right)^2. \tag{2.42}$$

The GVD due to material dispersion inside the prism material is

$$\Psi''_{M}(\lambda_0) = \frac{\lambda_0^3}{2\pi c^2}\frac{2\left(d + \left|\frac{dn}{d\lambda}\right|\Delta\lambda L\right)\sin\frac{\phi}{2}}{\cos\theta}\left.\frac{d^2n}{d\lambda}\right|_{\lambda_0}, \tag{2.43}$$

where d is the laser beam diameter. Then the total GVD of the prism pair is

$$\Psi''_{TOT}(\lambda_0) = \Psi''_{\alpha}(\lambda_0) + \Psi''_{M}(\lambda_0). \tag{2.44}$$

The dispersion can be doubled by use of four prism configuration described in the Figure 2.5. From formula (2.44) one can see that prism pair can also have positive dispersion if material dispersion is the dominant term, i.e. the distance between prisms is short. However, it is important to realize that if we work around the typical optical communication wavelength of 1550 nm, all glasses used to make prisms have anomalous dispersion. Therefore the configuration cannot give positive or zero dispersion values. This makes it sometimes unsuitable for dispersion compensation in these wavelength ranges.

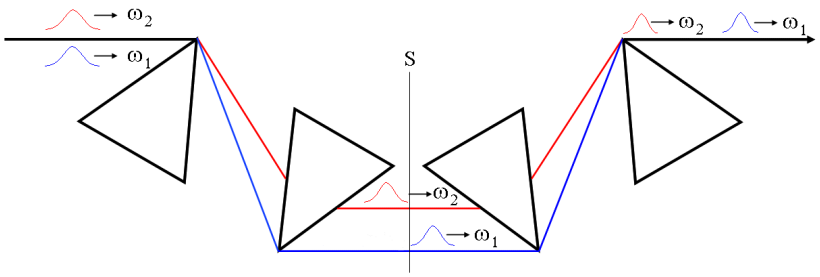

Figure 2.5: Four prisms aligned to induce negative group delay dispersion. Shorter wavelength ($\omega_1 > \omega_2$) pulses propagate thorough the system faster. S is the symmetry plane. The angle between blue and red component has been severely exaggerated and the distance between two prisms is usually much longer.

2.4.3 Grating pair

Gratings are diffractive elements that can produre much higher angular dispersion than prisms. However, they have considerable transmission losses (>20%) and this makes them often unsuitable for intracavity dispersion compensation in mode-locked lasers. On the other hand, they do not introduce nonlinear effects and hence are suitable when high power operation is required. Consequently, pulse compression with a grating pair has been extensively used [Tra69]. Typical grating configuration used to introduce anomalous GDD is presented in the Figure 2.6. The GDD of a grating pair is

$$\left.\frac{d^2\Psi}{d\omega^2}\right|_{\lambda_0} = -\frac{b\lambda_0^3}{2\pi c^2 d^2 \cos^3\beta'}, \tag{2.45}$$

where d is the grating constant, b is the normal separation between gratings and β' is the diffraction angle for the centre wavelength λ_0.

2.4.4 Chirped mirrors

Chirped mirrors are dielectric structures that consist of normal distributed Bragg reflector (DBR) on a substrate followed by a chirped DBR (CDBR). In a CDBR the centre wavelength of the stopband progressively decreases when going further away from the substrate. Thus a very broad optical bandwidth can be achieved. CDBR can be followed by a double-chirp

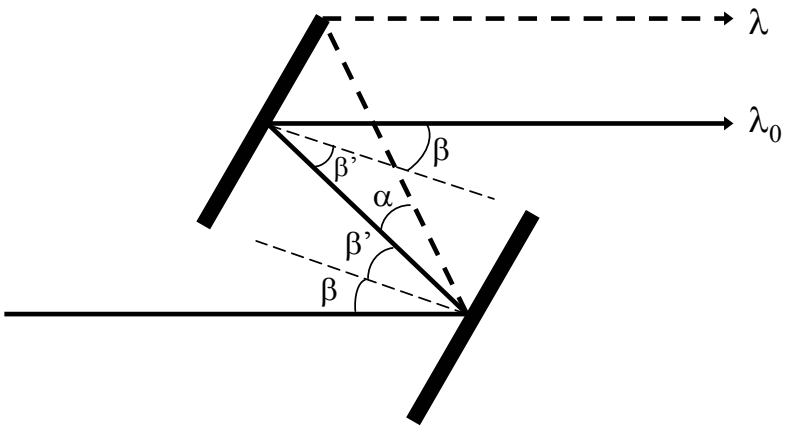

Figure 2.6: A grating pair producing negative group delay dispersion. $\alpha + \beta'$ is the diffraction angle for the wavelength λ.

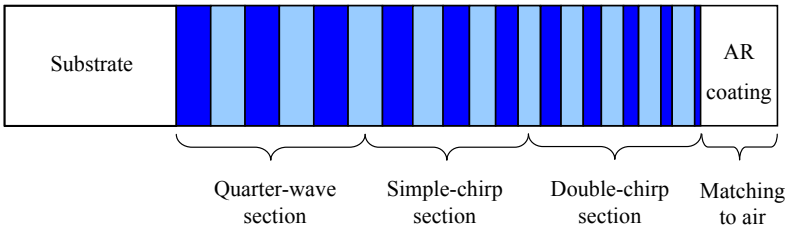

Figure 2.7: The general structure of a double-chirped mirror with index matching to air.

section ([KMS+97], [MKK98]) if compensation of the higher order dispersions is required. The entire structure should finally be matched to air with an anti-reflection coating. A typical structure of a double-chirped mirror is shown in the Figure 2.7.

Chirped mirrors [SFSK94] have enabled remarkable improvement in the field of generating ultra-short pulses. Their major benefits are low losses i.e. reflectivity over 99.8% [KMS+97], a large compensating bandwidth [MME+97], and a simple configuration.

Chirped mirrors can be designed to compensate several dispersion orders at the same time [MKK99]. However, they have known problems with matching the mirror refractive index to air. This index mismatch causes unwanted roughness in dispersion characteristics. Nonetheless, these problems can be reduced by operating the mirror from the substrate side

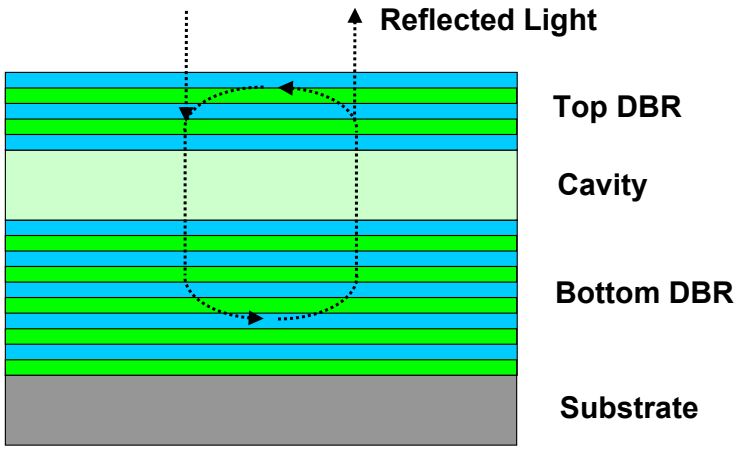

Figure 2.8: The basic structure of a Gires-Tournois interferometer.

and making the anti-reflection coating in the rear side of the component [MGS+00].

In spite of all these benefits, the chirped mirrors cannot be used for a broad range of applications where relatively high dispersion is required. GDD values of about $250 fs^2$ can be achieved over some tens of nanometer [SZM99]. GDDs of over $400 fs^2$ have been reported recently.

2.4.5 Gires-Tournois interferometer

A Gires-Tournois interferometer (GTI) consists of a partially reflective mirror, a cavity and a second mirror with 100% reflectivity [GT64]. The general concept of a dielectric GTI is presented in Figure 2.8. Such a structure ensures that various spectral components of an incident optical beam are reflected in equal proportion but they acquire a different group delay during reflection. In comparison with a prism pair, GTI structures can produce three orders of magnitude higher dispersion. The dispersion can be both negative and positive. However, it attains high values in a limited wavelength range. The operation bandwidth and the amount of dispersion can be accurately tuned by changing the reflectivity of the top reflector and the length of the GTI cavity. The top and bottom mirrors usually consists of a variable number of thin film layers, i.e. about 100 nm in thickness, with alternating high and low refractive indices that form a distributed Bragg reflector (DBR).

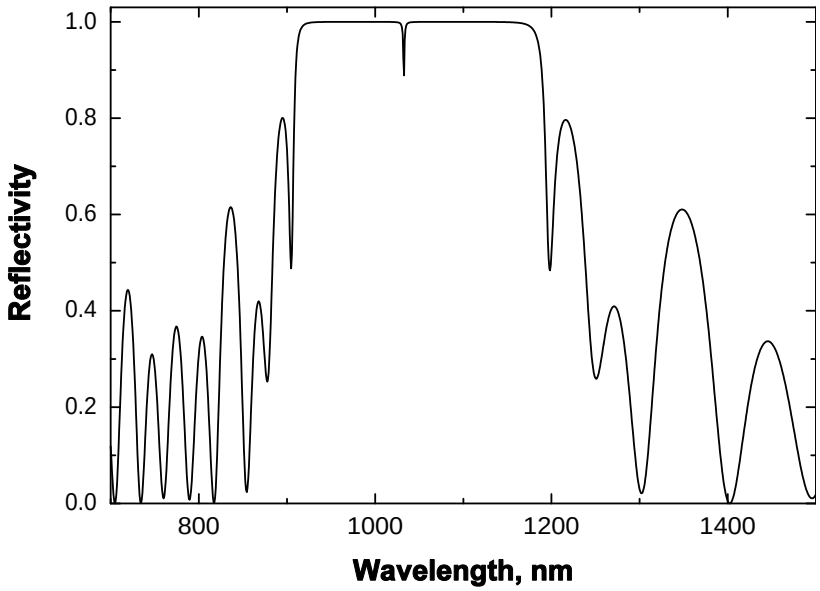

Figure 2.9: An example of a calculated GTI reflectivity spectrum with maximum dispersion of ± 0.05 ps^2.

The cavity introduces time delay to the propagating beam and its optical thickness determines the resonant frequencies. With a selected resonance wavelength λ, the cavity thickness, d, is a multiple of $\lambda/[2\cdot \mathrm{n}(\lambda)]$. However, high dispersion tends to yield losses near the resonant dip. Since we are interested in low loss components, we assume that bottom mirror has a reflectivity close to one and that the cavity material is lossless. In practice, this leads to use of dielectric material in near infrared region. With these assumptions we can simplify the expression [Iso03] for the phase of the reflected wave into a form:

$$\Phi(\omega) = \tan^{-1}\left(\frac{-(1-R)\sin(\varphi-\omega t_0)}{\sqrt{R}+(1+R)\cos(\varphi-\omega t_0)}\right), \tag{2.46}$$

where R is the top mirror reflectivity, φ is the phase change in GTI bottom mirror and t_0 is the round trip time of the interferometer. Now we preform a derivation to get the group delay (2.23) for a low loss GTI:

$$\tau_{GTI} = -\frac{d\phi}{d\omega} = -\frac{[1+R+\sqrt{R}\cos(\varphi-\omega t_0)](1-R)t_0}{[\sqrt{R}+(1+R)\cos(\varphi-\omega t_0)]^2+[(1-R)\sin(\varphi-\omega t_0)]^2}. \tag{2.47}$$

A Gires-Tournois interferometer can be made in many different ways. The bottom mirror can be metallic, semiconductor or dielectric. The cavity can be any transparent material or even air or vacuum. However, the manufacturing material has a strong influence on its properties, namely losses and bandwidth. Dielectric mirrors have the lowest losses because they can have the highest reflectivity in the bottom DBR. With semiconductor mirrors [Iso03] high dispersion values can be achieved but losses are high (>10%). Even with small dispersion values, such as $\pm 100 fs^2$, losses remain at 3.0% [LLDTJ98]. As a conclusion it is safe to say that dielectric GTIs provide the only compact means for a low loss high GDD generation for a laser cavity.

Dielectric GTIs are usually made with either electron beam evaporator or sputtering technique. The materials used in electron beam evaporation are mainly SiO_2 and TiO_2 which have the best mechanical and optical properties over large spectral range (0.4-2 μm): very low losses, almost constant refractive index, good adhesion, hard surface and small temperature dependence. SiO_2 is selected as a cavity material because it has the lowest absorbtion coefficient and is less dependent on oxygen partial pressure during evaporation than TiO_2.

One of the advantages of GTIs is that they can be designed to have a GDD of several ps^2; although at the expense of rather small compensation bandwidth. Typical compensation bandwidth for a dielectric GTI is few nanometers. This is sufficient for dispersion compensation of picosecond pulses. Another application for GTIs is optical pulse compression [KH86], [HSS03].

When we select a certain target GDD, GTI top mirror and cavity length should be numerically fitted using equations (2.47) and (2.26) to attain the required dispersion. However, it should be taken into account that the cavity thickness does not solely determine the resonance wavelength but also the top and bottom DBR induce some phase delay [BC92]. This resonance wavelength shift phenomena appears strongest when one increases the amount of top DBR pairs from only few to more than five pairs. The resonance dip shifts towards the DBR stopband centre. If broad and flat compensation bandwidth is needed, then the top mirror reflectivity should be low [WMJ98] (<70%) and the cavity thickness should correspond to one of the lowest resonance orders. However, this leads to low dispersion values, which is often against the original target.

2.5 Electron beam evaporation

Thin film technology is based on the fact that most pure materials form smooth layers when evaporated in vacuum conditions on a smooth surface. The motivation for producing thin films from optically transparent materials is that both high reflective and anti-reflective coatings are required to be lossless and of high performance. In addition, their transmission and reflectivity behaviour can be easily modelled with transfer matrix formalism as shown in section (2.2). In this thesis we mainly consider dielectric materials — they are almost entirely lossless in visible and near infrared region (from 500 nm to 2 μm).

The basic methods for vacuum deposition are [Pul84] sputtering and electron beam (EB) evaporation. Sputtering is based on high energy ions (e.g. Ar^+) colliding to a selected material and the formed heat evaporates the material. The vapor travels in vacuum or reactive gas (e.g. O_2) environment to target deposition surface and forms a thin material layer. A good example of sputtered material is TiO_2: Titanium (Ti) is evaporated with argon gun in oxygen (O_2) rich vacuum chamber and a film is formed with reaction: Ti + $O_2 \longrightarrow TiO_2$. This reaction requires elevated temperature and stable conditions in order to give homogenous refractive index over entire layer. This procedure gives not only TiO_2 but also other stoichiometric compounds like TiO and TiO_x.

Electron beam evaporator is a device, where pure elements or compounds are evaporated with high energy (4–10 keV) electrons. As consequence hot vapor propagates onto the target surface. Electron beam that heats the materials is generated with a hot filament source and electrons are made to travel circular path in vacuum because of a transversal magnetic field $\overline{B}$ that causes Lorentz force $\overline{F}$:

$$\overline{F} = m_e \overline{a} = e\overline{v} \times \overline{B}, \tag{2.48}$$

where m_e is the mass of the electron, e is the electron charge, $\overline{a}$ is the electron acceleration vector and $\overline{v}$ is the velocity. This configuration is described in the Figure 2.10.

The electron beam is focused and guided with fine tuned electric fields — both transversal orthogonal directions respect to velocity $\overline{v}$. The beam is very intense at material surface. It follows that the material surface heats up to thousands of kelvins. The flux of evaporated material is given by:

$$\Phi = 3.513 \cdot 10^{-22} \frac{P_{vapor}}{\sqrt{MT}} \frac{molecyles}{cm^2 s}, \tag{2.49}$$

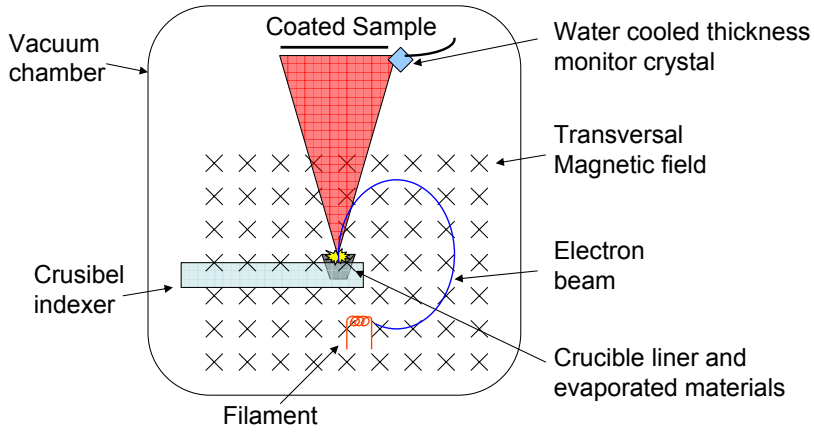

Figure 2.10: Electron beam evaporator configuration.

where P_{vapor} is the vapor partial pressure, M is the molecular mass and T is the gas temperature. Typical acceleration voltage is 6–10 kV, but for dielectric materials a slightly lower, 6–7.5 kV, is better. High energy electrons penetrate too deep into the dielectric materials and cause inhomogeneous material distribution over the target surface. Excessive acceleration voltage also consumes materials unnecessarily and may lead to damages in the evaporation system.

The electron beam evaporator has a shutter that either allows material flow to sample or blocks it totally. Other necessary equipment are thickness monitors, sample heaters, tilters and rotators, temperature monitors and ion-guns. Thickness monitor can be either optical or electrical. Optical methods are based on detection of a collimated beam and measuring either reflectivity spectrum or amplitude as a function of polarization angle. This allows use of ellipsometric techniques for calculating layer thicknesses and refractive indices. Electric method requires a gold coated quartz crystal oscillator. The crystal itself is a plano-convex plate, which is excited into thickness shear mode vibrations by the external oscillator at a frequency about 6 MHz. The frequency of the oscillation is determined by the mass of the material, which has been evaporated into the surface. As the deposit builds up so the oscillations slow down. The evaporated film thickness T_f can be calculated from the

following formula [Int02]:

$$T_f = \frac{D_q}{D_f} \frac{N_q T Z_f}{3.14\, Z_q} \tan^{-1} \frac{Z_q}{Z_f \tan\left(3.14\,(1 - T_q/T)\right)}, \tag{2.50}$$

where indices q and f stand for quartz and evaporated film, respectively, D is the density, T is the film thickness, N_q is the frequency constant for quartz crystal oscillating in thickness shear mode (Hz cm^{-1}), f is the frequency for loaded crystal and f_q for unloaded crystal and Z is the acoustic impedance.

Optical methods are more accurate than electro-mechanical but they are more difficult to perform in vacuum because of the need of sophisticated feedthroughs and difficult beam alignment. If optical methods are used, then often an electrical method is used simultaneously to keep track of the deposition rate and to be able to give fast feedback to electron gun power source. Constant deposition rate is one of the key parameters for keeping the deposition repeatable. Other environment issues are temperature, pressure, and for dielectric materials also the oxygen partial pressure. Ion-guns are used for cleaning the substrate surface before evaporation to reduce voids and contamination in the first boundary. During evaporation ion-guns can be used for ion assistance, which means that extra ions and molecules are brought to film surface. As an example, TiO_2 stoichiometry can be stabilized by introducing a constant low energy (20–50eV) O_2 flow with an ion-gun towards the sample during evaporation. Flow can also consist of neural molecules. This higher energy oxygen makes the thin film more dense, closer to bulk properties and reduces voids. Therefore such films can stand higher optical powers. In addition, also mechanical properties improve with most material: the film is smoother and more regularly organised and therefore harder.

In evaporation we want to avoid diffraction between evaporated molecules while they propagate to the sample. For this purpose we define mean free path, which is the longest distance that the molecule can travel on average in the vacuum pressure, p, and not collide between each other. Mean free path, h_f can be determined from the formula:

$$h_f = \left|\frac{5 \cdot 10^{-3}}{p(torr)}\right| cm = \left|\frac{6.7 \cdot 10^{-5}}{p(mbar)}\right| m, \tag{2.51}$$

where p is pressure, either in torr or mbar — both commonly used in vacuum technology (1 torr $\approx$ 133.322 Pa =1.33322 mbar). When we use formula (2.51), we find out that for typical high pressure electron beam evaporator situation (p$\approx 1.5 \cdot 10^{-4}$ mbar) the h_f is about 45 cm,

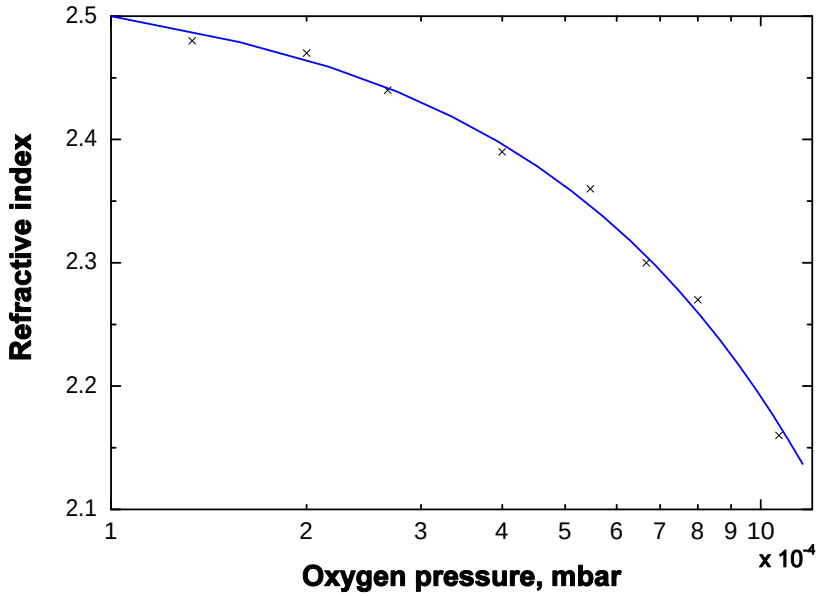

Figure 2.11: Dependence of the refractive index at 550 nm wavelength of TiO_2 films on the neural oxygen gas pressure during evaporation.

which is already of the same order as one will have between the sample and the evaporation source in real applications. However, for most materials and cases the pressure is of the order of 10^{-6}–$5 \cdot 10^{-5}$ mbar during evaporation, so mean free path is not always of concern.

In this thesis TiO_2 is used with every coating. Therefore it is important to describe its most important optical properties. Refractive index dependence on wavelength has been studied in various different evaporation conditions and the main characteristic feature of the material is that its refractive index depends strongly [Pul84] on oxygen partial pressure during evaporation. This phenomena is depicted in the Figure 2.11. Moreover, film properties also depend on oxygen ionization level: it has been shown that for many materials (SiO, SiO_2, BeO, La_2O_3, ZrO_2, In_2O_3, TiO, TiO_2) applying partially ionized oxygen to the evaporation process reduces absorption coefficient. Both refractive index and absorption coefficient can be determined with a spectroscopic ellipsometer.

The fact that increase of oxygen content decreases the refractive index in dielectric materials can be accurately modelled when extra oxygen amounts are small. By assuming

that molecules are randomly distributed over the layer, we can make a linear combination between refractive index given by dispersion formula (2.19) and void. This result sustains the layer thickness but propagating light undergoes decreased effective refractive index. In addition, accurate dispersion formula is also needed for fitting ellipsometric measurement data to real and complex refractive indices. If the oxygen content significantly increases during the evaporation, then the diffraction effects must be taken into consideration. In a thin film coating diffraction will appear as losses and reduced the structure performance.

Chapter 3

GTI fabrication and characterization

Gires-Tournois interferometers can be manufactured by various methods and they can be made of different kind of materials. Dielectric GTIs are commonly made by using either an electron beam evaporator or a sputtering technique. In this work all films were evaporated with custom designed Instrumentti Mattila electron beam evaporator. An ion-gun with both oxygen and argon gas sources was installed to the evaporation chamber and the sample holders could be either tilted or rotated inside the vacuum chamber. Most of the deposited films were evaporated using SiO_2 and TiO_2, which have the optimal mechanical and optical characteristics to ensure desired film properties. As a substrate, we have used n-doped GaAs or InP because of their high refractive indices and high absorption coefficients that help when performing ellipsometric measurements with thin substrates. Some of the coatings were deposited on Borofloat® glass. Those few samples were used in transmission as output couplers in a laser.

3.1 Calibration

Electron beam evaporators work at low pressure conditions providing layer thicknesses are of the order of 100 nm. This gives rise to issues of accuracy, repeatability and reliability.

Uncertainty in refractive indices and film thicknesses of the deposited layers limit the quality of the component. Properties also suffer due to possible voids and surface roughness. Therefore, these factors should be minimized before preforming the actual evaporation.

Film thickness is monitored optically in industrial EB-systems but we have settled to crystal thickness monitoring. This means that we have to learn first how the selected materials behave, grow test films and measure their properties. These measurements are then used to calibrate evaporation process.

Evaporation conditions are mainly based on experience gathered over the years and some publications [Jea98] but one must always remember that there are still differences between every EB-system even if they seem to be exactly the same. We have systematically tested different operation conditions since the installation of the device in June 2002. Laboratory temperature and especially humidity in the summer time seem to affect the performance. Moist slows down the pump-down time and the extra water molecules in the chamber increase the amount of voids or oxygen content in TiO_2 films.

3.1.1 Thickness calibration

Thickness calibrations are performed before evaporating thin films that require precise parameters after loading new materials or after changing the evaporation conditions. The operation can be summarized in a few major steps:

1. Load a small piece of substrate to the chamber and set the intended evaporation conditions: pressure (oxygen or air), temperature, rotation speed and right EB-current and voltage for the material in use.

2. Evaporate a thin film with thickness e.g. 80.0 nm with selected deposition rate. For example for SiO_2 0.2 nm/s is quite common for thicker samples. Keeping the conditions stable usually needs active adjustments.

3. Unload the test sample and measure its thickness with an ellipsometric method. Simple single wavelength tools (we used Rudolf Research AutoEL III -ellipsometer at 632.8 nm) can give a reasonable accuracy for certain lossless films. However, in general, spectroscopic ellipsometer is needed to determine the thickness and refractive index at the same time.

4. Based on the measurements calculate and set the tooling factor into the thickness monitor.

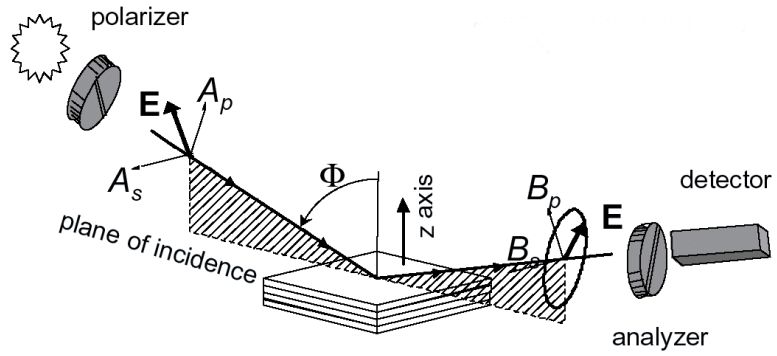

Figure 3.1: A spectroscopic ellipsometer configuration.

5. Repeat the previous steps for all the materials that will be used or to prove whether the oxygen content has stabilized for newly loaded materials.

3.1.2 Refractive index measurement

Refractive index is a key property of an optical material. Therefore, knowing the refractive indices of the materials at the wavelengths of interest is always valuable information. Initially, to determine the refractive indices, we used a single wavelength ellipsometer. The refractive indices for other wavelengths were calculated using dispersion formulas. After installation of a SOPRA GES5 spectroscopic variable angle ellipsometer, we were then able to determine directly both real and complex refractive indices [S.A97] of our dielectric materials. The basic configuration of the device is described in the Figure 3.1.

Ellipsometer measures surface reflectivities for different polarization angles and for different wavelengths. Based on these measurements, ellipsometric parameters $\tan\Psi$ and $\cos\Delta$ were extracted for each wavelength and were used to determine the refractive indices numerically. Our software uses Levenberg-Marquardt-algorithm [S.A97] for this numerical calculation. If too many fitting parameters are used in optimization algorithm and initial values are far from actual values, there is a possibility that algorithm converges to a local mathematical minimum [Kal02] that is not physically possible.

Refractive index measurements we performed among others for GaAs, SiO_2 and TiO_2.

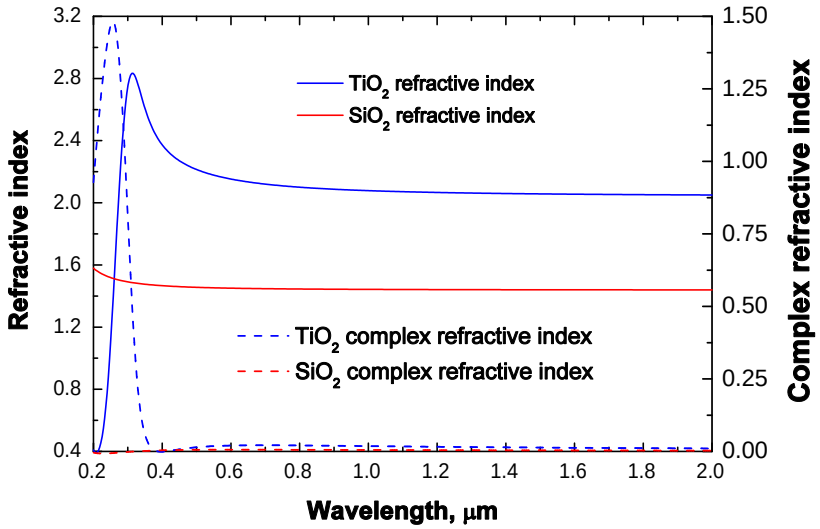

Figure 3.2: Measured refractive index values for SiO_2 and TiO_2. SiO_2 had 0.2 nm/s evaporation rate at oxygen pressure of $3.0 \cdot 10^{-5}$ mbar, for TiO_2 the rate was 0.1 nm/s at $1.5 \cdot 10^{-4}$ mbar.

In the Figure 3.2 we present an example of such refractive index measurement results. These data were used for designing an anti-reflection coating for a semiconductor laser facets.

3.2 GTI design procedure

Before one can evaporate any sensible mirrors, one must design them. The basic structures were described in the previous chapter and after calibrations we know the refractive indices for used materials.

Although many thin films were made, we present here just a few examples in detail. Other similar films can be made by adjusting the design parameters, like target wavelength and target dispersion. For a Gires-Tournois interferometer we first need a DBR that has a stopband center wavelength, λ_c. The resonance wavelength of a GTI should be located within hte stopband of the DBR. Our GTI was intended to operate with an Ytterbium fibre laser. Therefore, the first target wavelength was set to 1050 nm.

The bottom DBR is a highly reflective mirror. We used for a DBR 10 pairs of SiO_2 and TiO_2 on top of a GaAs substrate. This gives about 99.89 % reflectivity at the λ_c. One layer

in a DBR is a quarter of the λ_c, therefore each layer thickness is $\lambda_c/(4n(\lambda_c))$.

The parameters that also need to be adjusted in a GTI are the cavity thickness and top DBR reflectivity. They must be considered together because they determine the dispersion properties and optical bandwidth. Using formulas 2.47 and 2.26 we can numerically iterate the desired dispersion. Here we must take into account the fact that we have certain limitations in our thickness monitoring and very thick cavities cannot be accurately positioned. For this reason we selected the cavity thickness to be λ_c. The number of the top DBR pairs was set to 4.5 and providing anomalous dispersion that would compensate the fibre laser cavity dispersion. Dispersion calculations are based on equations (2.47) and (2.26). The top mirror reflectivity for different number of pairs is given by equation (2.18). This set of GTI parameters results in a small net anomalous GVD. Contrary to our expectations and owing to uncertainty in the deposition process, the first experimental trials has given a resonance wavelength of 1023 nm. Calculated reflectivities at maximum anomalous dispersion wavelength, 1022.8 nm, are R=0.9356 for the top DBR and R=0.9989 for the bottom DBR.

3.3 Evaporation procedure

The evaporation of a thin film is usually automated with computers. However, our evaporator does not have such automation and this leads to a bit lower repeatability. On the other hand, this gives the possibility to tune the conditions actively based on visual observations when materials become exhausted at some spot of the crucible liner. The beam can be moved to a new optimum path to compensate the irregular consumption.

Because evaporation routines vary from one machine to another we, do not describe all the steps here, but instead made an appendix A for operating instructions for our Instrumentti Mattila electron beam evaporator that includes roughly all the steps and details for successful evaporation. Evaporation conditions were kept constant during evaporation: extra oxygen was supplied to the chamber and pressure was kept at $3 \cdot 10^{-5}$ mbar for SiO_2 with rate of 0.2 nm/s and $1.5 \cdot 10^{-4}$ mbar for TiO_2 with rate of 0.1 nm/s. The chamber background pressure was less than $5 \cdot 10^{-6}$ mbar. Table 3.1 shows an example of a 10 pair 1050 nm DBR evaporated on a semi-insulating (SI) GaAs substrate.

Table 3.1: An example of evaporation conditions for a 10 pair 1050 nm DBR deposited on SI-GaAs substrate. TF is the tooling factor, p is the pressure, T is the sample holder temperature measured with an infrared detector. The emission current is shown in the table while the acceleration voltage was kept at 7.5 kV. Rate is given by the Intellimetrics thin film monitor. Usage describes the amount of mass deposited on the crystal. Usage numbers are given here after each deposited layer. After usage values of about 140 the crystal no longer vibrates stably.

Material	Thickness, nm	TF	p, mbar	T, °C	Current, mA	Rate, nm/s	Usage
SiO_2	181.0	1.10	$3.0 \cdot 10^{-5}$	90.6	20–23	0.2	25.56
TiO_2	122.1	1.55	$1.5 \cdot 10^{-4}$	91.1	100–93	0.1	28.29
SiO_2	181.0	1.10	$3.0 \cdot 10^{-5}$	90.0	20	0.2	31.23
TiO_2	122.1	1.55	$1.5 \cdot 10^{-4}$	90.5	95–100	0.1	34.02
SiO_2	181.0	1.10	$3.0 \cdot 10^{-5}$	89.4	20	0.2	36.96
TiO_2	122.1	1.55	$1.5 \cdot 10^{-4}$	91.2	107	0.1	39.74
SiO_2	181.0	1.10	$3.0 \cdot 10^{-5}$	90.2	33	0.2	42.67
TiO_2	122.1	1.55	$1.5 \cdot 10^{-4}$	90.7	100	0.1	45.45
SiO_2	181.0	1.10	$3.0 \cdot 10^{-5}$	88.6	20	0.2	48.4
TiO_2	122.1	1.55	$1.5 \cdot 10^{-4}$	90.8	121	0.1	51.14
Changed to the second SiO_2 source.							
SiO_2	181.0	1.10	$3.0 \cdot 10^{-5}$	90.1	17	0.2	54.07
TiO_2	122.1	1.55	$1.5 \cdot 10^{-4}$	90.8	127	0.1	56.82
SiO_2	181.0	1.10	$3.0 \cdot 10^{-5}$	90.1	16–18	0.2	59.75
TiO_2	122.1	1.55	$1.5 \cdot 10^{-4}$	90.4	120	0.1	62.5
SiO_2	181.0	1.10	$3.0 \cdot 10^{-5}$	89.5	17	0.2	65.42
TiO_2	122.1	1.55	$1.5 \cdot 10^{-4}$	91.1	124	0.1	68.21
SiO_2	181.0	1.10	$3.0 \cdot 10^{-5}$	90.3	18	0.2	71.13
TiO_2	122.1	1.55	$1.5 \cdot 10^{-4}$	91.2	120	0.1	73.85
SiO_2	181.0	1.10	$3.0 \cdot 10^{-5}$	89.9	19	0.2	76.8
TiO_2	122.1	1.55	$1.5 \cdot 10^{-4}$	91.5	115–110	0.1	79.48

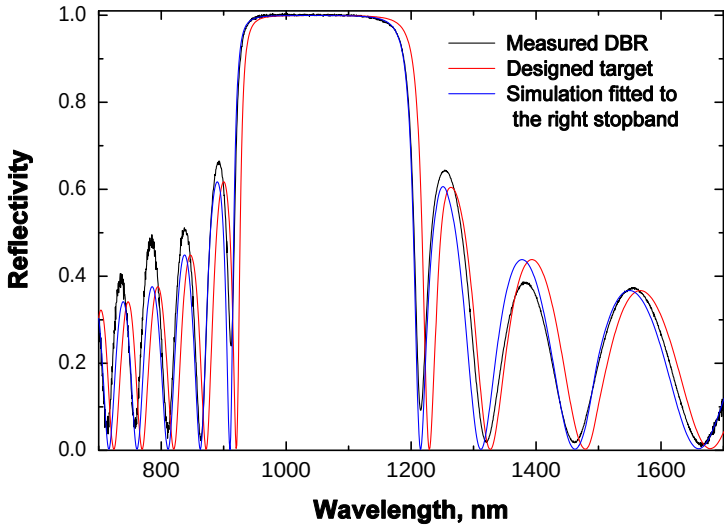

Figure 3.3: Reflectivity spectrum of the bottom DBR that was produced to operate at the 1.05 μm GTI. The black line is the measured spectrum, the red one is the original desing and the blue one is the original target shifted -12nm to match the measured spectrum stopband center.

3.4 Measurements of thin film mirrors

We would like to note, that measuring the absolute value of a film reflectivity accurately is a challenging task, especially near the low or the high reflectivity limits. Often the reflectivities near these limits has to be known with high precision.

Reflectivity spectrum usually reveals accurate information about dielectric mirror's properties. This is why we always first perform a reflectivity measurement for a mirror prior to any other tests. Reflectivity was measured in several ways but mainly with a RPM2000 Compound Semiconductor PhotoLuminesence System that operates in visible and near infrared region [RPM00]. For measurements in 1–1.8 μm wavelength range a gold mirror was used as a reference mirror to extract absolute values of reflectivity. In the Figure 3.3 we present the measured reflectivity for a DBR that acted as a bottom mirror for our 1023 nm GTI. After depositing the cavity and top DBR, the GTI structure was completed with the reflectivity shown in the Figure 3.4.

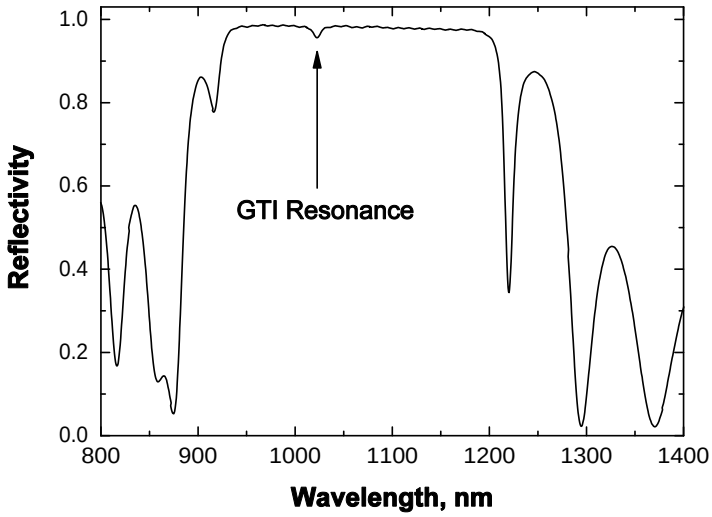

Figure 3.4: Reflectivity spectrum of the sample GTI15032003#3. The resonance dip can be seen clearly at 1023 nm. GTI sidebands are asymmetric because the bottom and top DBRs are positioned at different stopbands.

3.5 Dispersion measurements

The GDD of a fabricated $\sim 1.5\mu$m GTI was measured indirectly by measuring first the group delay. A tunable laser near 1570 nm wavelength was used as probe and the group delay was analyzed using conventional phase-shift method. The principle of this dispersion measurement technique is explained in [Der98]. The setup we used was originally build to measure the GDD of semiconductor GTIs [Iso03]. However, the accuracy of this system was not enough for measuring low values of group delays typical for dielectric GTIs. To generate sufficient amount of group delay, we have used top DBR with relatively high value of reflectivity. This led to increased losses of the GTI near the resonant wavelength due to limited reflectivity of the the bottom DBR consisted only of 8 pairs of SiO_2 and TiO_2. As a result we could reliably detect the change with the group delay near the resonant wavelength. The results are presented in the Figure 3.5. Top and bottom mirror reflectivities were fitted to the group delay and reflectivity models simultaneously. Those parameters were then used to calculate GDD and dispersion parameter shown in the Figure 3.6.

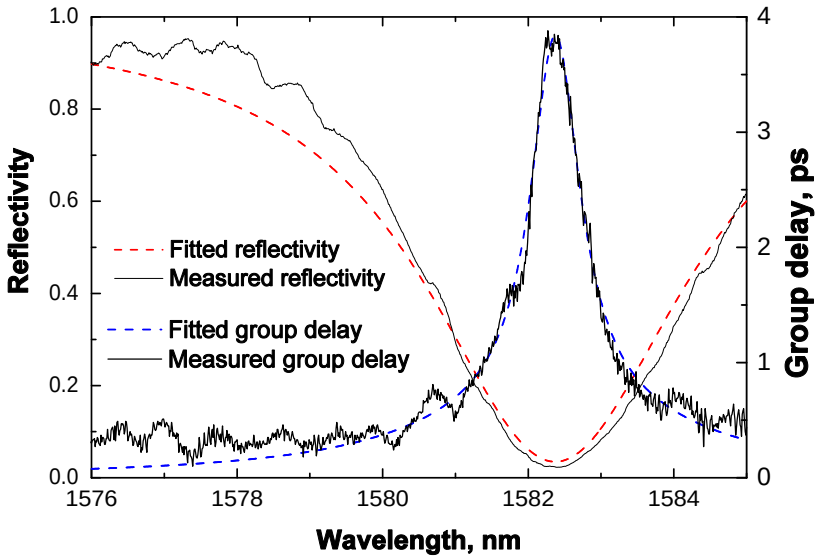

Figure 3.5: The reflectivity and group delay for a high loss GTI.

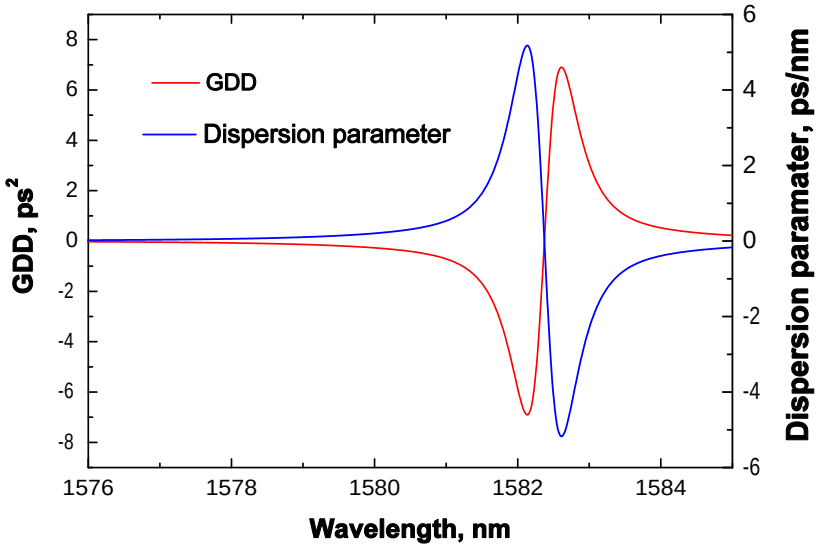

Figure 3.6: GDD and dispersion parameter for a high loss GTI.

Chapter 4

Results and conclusions

4.1 Testing a GTI in a fibre laser cavity

The GDD of the fabricated 1 μm-GTIs could not be measured directly using available dispersion measurement systems. This is due to a lack of proper tunable laser in 1 μm region. The GTI dispersion was estimated based on the reflectivity spectrum. To prove that the GTI operates at the negative GDD we used the GTI as a cavity mirror in a fibre laser, as shown in the Figure 4.1.

A highly-doped Yb-fibre and a short segment of a single-mode fibre were contained in the cavity providing a low value of net normal GVD. This allows to implement a GTI mirror with a comparable amount of anomalous dispersion. The GTI dispersion is designed to generate a net anomalous dispersion that is slightly higher than the normal dispersion of the cavity in order to preserve sufficient optical bandwidth for supporting picosecond pulses. Adding one more pair to the top DBR would produce higher dispersion, but the bandwidth would be somewhat smaller. Linear cavity is defined by the semiconductor saturable absorber mirror (SESAM) used to initiate mode-locked operation and the GTI reflector.

An ytterbium-doped silica fibre (NA=0.22 and cutoff wavelength is 910 nm) has the unsaturated fibre absorption at 977 nm of $\sim$1900 dB/m. The Yb-fibre was manufactured using direct nanoparticle deposition (DND) technology [TKS$^+$02]. This fibre allowed us to keep the total length of the fibre within the cavity small. Overall fibre length was about 74 cm.

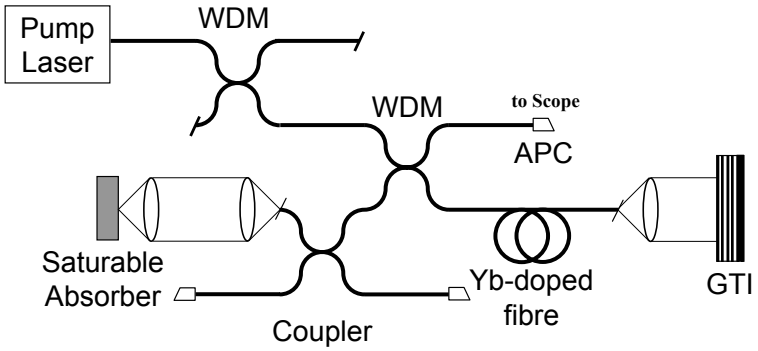

Figure 4.1: A fibre laser setup with a GTI acting as a dispersion compensating element.

The Yb-fibre was core-pumped through a 915/1000 nm fibre multiplexer with a maximum fibre-coupled pump power of 130 mW at 915 nm. Fibre splitter couples ∼10% of the power to the output. All fibre components had a cutoff wavelength of ∼910 nm. A broadband SESAM structure operating in 940–1050 nm wavelength range based on GaInNAs material system was monolithically grown by all-solid-source molecular beam epitaxy on an n-type GaAs (001) substrate and was similar to the long-wavelength SESAM described in [OJK$^+$03]. The sample includes bottom mirror comprising 25 pairs of AlAs and GaAs quarter wave layers forming a DBR with a center wavelength of ∼1000 nm. An antiresonant Fabry-Pérot structure of SESAM is formed by the uncoated front surface, multiple quantum-well (MQW) GaInNAs absorber and the highly reflecting AlAs/GaAs mirror stack [KdAK98]. Important feature of this GaInNAs-based SESAM is high contrast in nonlinear reflectivity variation (∼8%), as demonstrated in the [OJK$^+$03]. This absorber property allows to trap reliably the pulse spectrum at the regime with anomalous GVD. MQW layers of the SESAM were implanted with doses of $10^{12} cm^{-2}$ of 10 MeV Ni-ions.

4.2 Fibre laser performance with a GTI

The GTI performance was characterized based on the performance of the fibre laser with the GTI as a dispersion compensator. The laser threshold for continuous wave operation was about 15 mW. When the Yb-doped fibre length was ∼ 2.5 cm, the central lasing wavelength

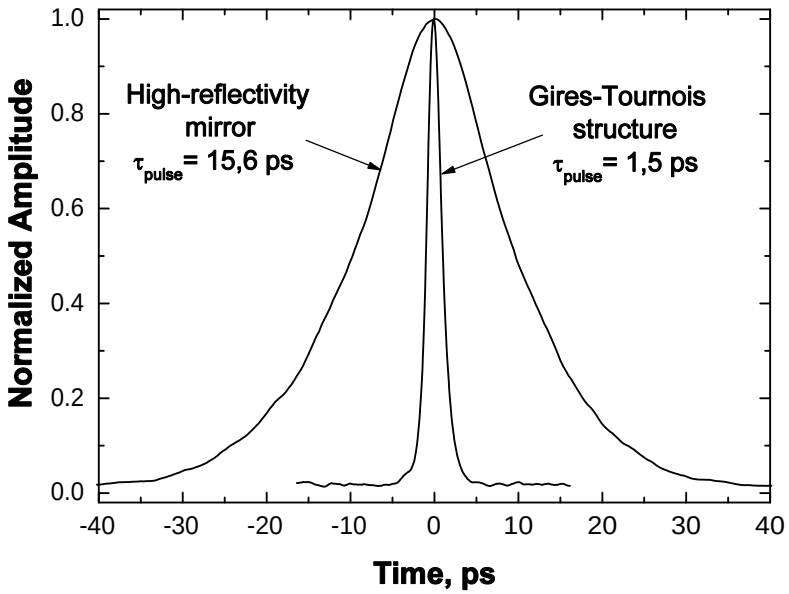

Figure 4.2: Measured autocorrelator traces for laser output with and without GTI.

was within the range of 1020-1030 nm. With shorter lengths of Yb-fibre, the laser was operating at 980 nm.

Self-started mode-locked operation at spectral range around λ=1023 nm with anomalous GVD was obtained for pump power above 40 mW with the output power up to $\sim$1 mW. Figure 4.2 illustrates autocorrelations for laser operating with a GTI reflector and with GTI replaced by an ordinary highly reflective metallic mirror. The pulse durations were 1.5 and 15.6 ps, respectively, assuming a Gaussian pulse shape. Comparison of the autocorrelations shows that GTI provides significant compensation for the fibre dispersion. Implementing of the GTI resulted in pulse shortening by a factor of the order of 10. The fundamental cavity frequency pulse train was 95 MHz.

Figure 4.3 shows GTI reflectivity and the resultant GVD around the resonance, and pulse spectra with GTI and with a highly-reflective metallic mirror used instead of GTI. The negative GVD of approximately -0.05 ps^2 is generated by GTI at the laser wavelength. The total dispersion in the cavity, including a double pass of fibre segment and GTI, were estimated to be -0.01 ± 0.005 ps^2. The estimation shows that the total cavity dispersion

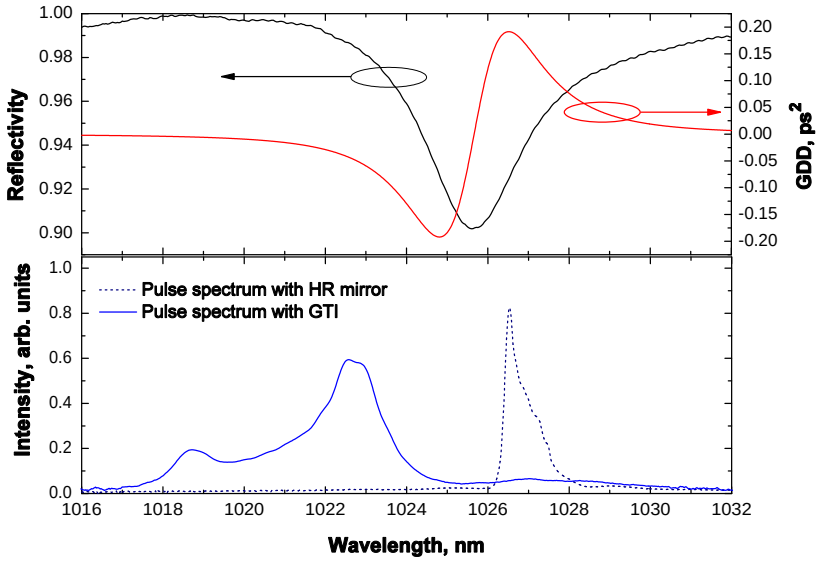

Figure 4.3: Reflectivity of a manufactured GTI near the resonance wavelength and calculated group delay dispersion based on reflectivity measurements. Lower curves are pulse spectra for cases, where laser was operated first with a high reflective metallic mirror and then with the GTI.

corresponds to a small net anomalous group-velocity dispersion. The uncertainty in the cavity dispersion relates to the problem with estimation of the dispersion of the highly-doped Yb-fibre. It is important to note, that using a SESAM with high contrast of nonlinear reflectivity, the operation in the negative GVD regime near $\lambda = 1022.8$ nm was possible without any wavelength-selective elements despite the reflectivity dip around GTI resonant wavelength. Mode-locked operation runs at this wavelength spontaneously for sufficient pumping power.

4.3 Conclusions

We have demonstrated that dielectric Gires-Tournois interferometers can be manufactured with an electron beam evaporator and used in a mode-locked 1022.8 nm Yb-fibre laser to compensate the intracavity dispersion. The laser is compact and easy to align because the laser has a tendency to work at GTI's negative dispersion slope. When comparing this

method to conventional dispersion compensation methods available at these wavelengths, we can see that GTI-based dispersion compensator allows for an anomalous dispersion and low losses. A GTI demonstrates good performance as a dispersive mirror yet lacking wavelength tunability. However, the lack of tunability results in a very high stability for the resonance wavelength. As a conclusion, I claim that dielectric GTIs provide a compact means for providing a low loss high GDD for a laser cavity at a selected wavelength.

Chapter 5

Summary

In this work we have demonstrated that dielectric Gires-Tournois interferometers can be manufactured with an electron beam evaporator and used in a mode-locked Yb-fibre laser to compensate the intracavity dispersion. The cavity is compact and easy to align. We have found out that the laser has a tendency to work at GTI's negative dispersion slope. As a result, overall anomalous group-velocity dispersion was obtained by using short length cavity with highly-doped Yb-fibre and dielectric Gires-Tournois compensator. As a conclusion I claim that dielectric GTIs provide a compact means for providing a low loss high GDD for a laser cavity at selected wavelength.

Using a broadband semiconductor saturable absorber mirror based on GaInNAs material system with large change in nonlinear reflectivity, we obtained self-started 1.5 ps pulse mode-locked operation at 1022.8 nm with a repetition rate of 95 MHz. This shows that high reflective Gires-Tournois mirrors are a promising alternative to grating pairs for controlling intracavity dispersion in fibre lasers. These results were submitted to Applied Optics in May 2003. Attaining such short pulses proves that this work has achieved its targets and enables us to proceed deeper into the subject.

In the future we are going to use Gires-Tournois interferometers in even shorter wavelengths in order to extend the possible applications of this type of fibre laser. Further studies will also include detailed dispersion measurements of the dielectric and semiconductor dispersive mirrors.

Bibliography

[Agr97] G. P. Agrawal. *Fiber-Optic Communication Systems*. John Wiley & Sons, Inc., New York, NY, 2nd edition, 1997.

[Agr01] Govind P. Agrawal. *Nonlinear Fiber Optics*. Academic Press, Sandiego, CA, 3rd edition, 2001.

[BC92] Dubravko I. Babic and Scott W. Corzine. Analytic expressions for the reflection delay, penetration depth, and absorptance of quarter-wave dielectric mirrors. *IEEE J. Quantum Electronics*, 28(2):514–524, February 1992.

[BWK91] M. Beck, I. A. Walmsley, and J. D. Kafka. Group delay measurements of optical components near 800 nm. *IEEE J. Quantum Electronics*, 27(8):2074–2081, 1991.

[CBJS86] D. N. Christodoulides, Etan Bourkoff, Richard I. Joseph, and T. Simos. Reflection of femtosecond optical pulses from multiple-layer dielectric mirrors -analysis. *Transactions on Quamtum Electronics*, QE-22(1):186–191, January 1986.

[Der98] Dericson, D. (ed.). *Fiber optic test and measurement*. Prentice Hall, NJ, 1998.

[FMG84] R. L. Fork, O. E. Martinez, and J. P. Gordon. Negative dispersion using pairs of prisms. *Opt. Lett.*, 9(5):150–152, February 1984.

[GT64] F. Gires and P. Tournois. Interféromètre utilisable pour la compression d'impulsions lumineuses modulées en fréquence. *C. R. Acad. Sci.*, 258:6112–6115, 1964.

[Hec98] E. Hecht. *Optics*. Addison-Wesley, Massachusetts, 3rd edition, 1998.

[HSS03] M. Hacker, G. Stobrawa, and R. Sauerbrey. Femtosecond-pulse sequence compression by Gires-Tournois interferometers. *Opt. Lett.*, 28(3):209–211, 2003.

[Int02] Intellemetrics. *IL150 Quartz Crystal Rate Monitor, application Instructions*. Intellemetrics Ltd., Clydebank, UK, 2002.

[Iso03] Antti Isomäki. Semiconductor mirrors for optical noise suppression and dispersion compensation. Master's thesis, Tampere University of Technology, Tampere, March 2003.

[Jea98] Lee. Jungkeun and et. al. Novel design procedure of broad-band multilayer antireflection coatings for optical and optoelectronic devices. *Journal of Lightwave Technology*, 16(5), May 1998.

[Kal02] Osmo Kaleva. Matemaattinen optimointi 1. http://butler.cc.tut.fi/∼kaleva/Mot1.pdf, Tampere University of Technolgy, May 2002.

[KdAK98] F. X. Kärtner, J. Aus der Au, and U. Keller. Mode-locking with slow and fast saturable absorbers -what's the difference? *IEEE J. of Selected Topics in Quantum Electronics*, 4:159–168, 1998.

[KH86] Jürgen Kuhl and Joachim Heppner. Compression of femtosecond optical pulses with dielectric multilayer interferometers. *IEEE Trans. Quantum Electronics*, 22(1):182–185, 1986.

[KMS+97] F. X. Kärtner, N. Matuschek, T. Schibili, U. Keller, H. A. Haus, C. Heine, R. Morf, V. Scheuer, M. Tilsch, and T. Tschudi. Design and fabrication of double-chirped mirrors. *Opt. Lett.*, 22(11), June 1997.

[LLDTJ98] M. J. Lederer, B. Luther-Davies, H. H. Tan, and C. Jagadish. An antiresonant Fabry-Pérot saturable absorber for passive mode-locking fabricated by metal-organic vapor phase epitaxy and ion implantation design, characterization, and

mode-locking. *IEEE J. Quantum Electronics*, 34(11):2150–2161, November 1998.

[MGS+00] N. Matuschek, L. Gallmann, D. H. Shutter, G. Steinmeyer, and U. Keller. Back-side-coated chirped mirrors wih ultra-smooth broadband dispersion characteristics. *Appl. Phys. B*, 71:509–522, 2000.

[MKK98] N. Matuschek, F. X. Kärtner, and U. Keller. Theory of double-chirped mirrors. *IEEE Journal of Selected Topics in Quantum Electronics*, 4(2), 1998.

[MKK99] N. Matuschek, F. X. Kärtner, and U. Keller. Analytical design of double-chirped mirrors with custom-tailored dispersion characteristics. *IEEE J. Quantum Electronics*, 35(2), February 1999.

[MME+97] E. J. Mayer, J. Möbius, A. Eutaneuer, W. W Rühle, and R. Szipőcs. Ultrabroadband chirped mirrors for femtosecond lasers. *Opt. Lett.*, 22(8), April 1997.

[Nie02] Tapio Niemi. *Dispersion measurements of fiber-optic components and applications of a novel tunable filter for optical communications*. PhD thesis, Helsinki University of Technology, Espoo, 2002.

[OJK+03] O. G. Okhotnikov, T. Jouhti, J. Konttinen, S. Karirinne, and M. Pessa. 1,5 μm monolithic GaInNAs semiconductor saturable-absorber mode locking of an erbium fiber laser. *Opt. Lett.*, 28(5):364–366, 2003.

[Pul84] Hans K. Pulker. *Coatings on Glass*. Elsevier, New York, 1984.

[RPM00] *RPM2000 Compund Semiconductor PhotoLuminesence System User Manual*. Accent Optical Technologies Ltd., Hertfodshire, England, 2000.

[S.A97] SOPRA S.A. *Winelli version 4.07*. France, April 1997.

[Saa02] Mika Saarinen. *Visible Vertical-Cavity Light Emitters*. PhD thesis, Tampere University of Technology, Tampere, September 2002.

[Sav92] Pekka Savolainen. Puolijohdelasereiden peilipäätyjen pinnoitus. Master's thesis, Tampere University of Technology, 1992.

[SFSK94] R. Szipőcs, K. Ferencz, C. Spielmann, and F. Krausz. Chirped multilayer coatings for broadband dispersion control in femtosecond lasers. *Opt. Lett.*, 19(3):201–203, February 1994.

[Sin98] Juha Sinkkonen. *Kvanttielektroniikka*. Helsinki University of Technology, Espoo, 1998.

[Sve98] O. Svelto. *Principles of Lasers*. Plenum Press, New York, NY, 4th edition, 1998.

[SZM99] R. A. Steven, Zhang Zhigang, and Ogura Mutsuo. Highly dispersive mirror in Ta_2O_5/SiO_2 for femtosecond lasers designed by inverse spectral theory. *Applied Optics*, 38(21), July 1999.

[THF+99] Hiroyuki Toda, Kazunori Hamada, Yasushi Furukawa, Yuji Kodama, and Shigeyuki Seikai. Experimental evaluation of gordon-haus timing jitter of dispersion managed solitons. In *25th European Comference on Optical Communication (ECOC'99), P3.18*, volume 1, pages 406–407, 1999.

[TKS+02] S. Tammela, P. Kiiveri, S. Särkilahti, M. Hotoleanu, H. Valkonen, M. Rajala, J. Kurki, , and K. Janka. Direct nanoparticle deposition process for manufacturing very short high gain Er-doped silica glass fibers. In *Proc. ECOC'02*, volume 4, page paper 9.4.2, 2002.

[Tra69] Edmond B. Tracy. Optical pulse compression with diffraction gratings. *IEEE J. Quantum Electronics*, 5(9):454–458, September 1969.

[WMG+02] P. C. Wagenblast, U. Morgner, F. Grawert, T. R. Schibli, F. X. Kärtner, V. Scheuer, G. Angelow, and M. J. Lederer. Generation of sub-10-fs pulses from a kerr-lens mode-locked Cr^{3+}:LiCAF laser oscillator by use of third-order dispersion-compensating double-chirped mirrors. *Opt. Lett.*, 27(19), October 2002.

[WMJ98] Niklaus U. Wetter, Edison P. Maldonado, and Nilson D. Vieira Jr. Calculations for Broadband Intracavity Chirp Compensation with Thin-Film Gires-Tournois

Interferometers. *Revista de Física Aplicada e Instrumentação*, 13(2):31–33, 1998.

[Yeh88] Pochi Yeh. *Optical Waves in Layered Media*. Wiley, New York, 1988.

[Zha02] Xinping Zhang. *High-repetition-rate Femtosecond Optical Parametric Oscillators Based on KTP and PPLN*. PhD thesis, Phillipps-Univesität Marburg, Marburg/Lahn, Germany, October 2002.

Appendix A

Operation instructions for EB-system

Instrumentti Mattila electron beam evaporator operation instructions, version 1.4 by Lasse Orsila, 16.5.2003

Loading samples

1. Open the cold (label CHAMBER COLD IN) and hot water (label CHAMBER HOT IN) valves below windows. Remember that if you are going to evaporate then you also need to open water valve for electron gun cooling (label GUN WATER IN).
2. Turn the WATER knob to HOT position in control panel.
3. Wait until the loading chamber is hot and then press upper red STOP -button. This will close the valve between the loading chamber and electron beam gun chamber.
4. Open upper nitrogen valve (V5) and wait until the chamber pressure reaches $1.0 \cdot 10^3$ mbar (1 atm).
5. Open the chamber lid upwards and insert the samples.
6. Rotate the sample holder so that samples are facing down.
7. Close the chamber lid and close the nitrogen valve (V5).

8. Press the upper green PUMP -button to start pumping down the chamber. Change to cold water when you reach pressure lower than $1.0 \cdot 10^{-4}$ mbar. Make sure that you have opened all cold-water valves (Gun cooling water, cold water for the chamber) if you are going to evaporate.

Evaporating thin films

1. When you have reached $7 \cdot 10^{-5}$ mbar pressure you can start preparing your evaporation: open the gun water line and make sure that you have sufficient flow, open also the chamber cold water line.

2. You have to prepare evaporation conditions: Select the proper layer number (1–4) from the thickness monitor (see table A.1 for materials and layer numbers) and set some typical value for the tooling factor (TF); if you do not know what TF to expect, leave the value for its current value. Select the correct crucible position by using the feedthrough on the rear side of the chamber. Use the sample heater to heat your sample to some stable temperature, usually set T=90.0 °C and turn on the cold water for the chamber; if you use the rotating sample holder, temperature should be higher due to the fact that measurement system monitors a different surface.

3. When the chamber wall is cold, T is about 90 °C and the pressure below $2 \cdot 10^{-5}$ mbar, you can turn on the MAIN POWER from the Telemark power supply (green button on the left).

4. Turn on the HIGH VOLTAGE (do not change any settings).

5. Open the oxygen gas line valve (before T-bloc, reads AGA on top of it, plastic O2-label next to it) about 90 ° degrees counter clockwise (=fully open).

6. Turn on SOURCE (current must be 0 mA at this point, if not then turn the current off and turn the knob counter clockwise to zero value and turn the current on again)

7. Select the right beam shape (spiral for SiO_2 and manual for TiO_2 and Ti_3O_5)

8. Increase the current to 5–10 mA and look at the beam: move the beam to the centre of the crucible liner (there should be enough material left!) by using the joystick at the

separate control box (for this you must be trained, misuse will destroy the liner and electron beam gun!)

9. Increase the current to estimated operation value (see parameter table A.1)
10. Set the pressure to target value (see parameter table A.1) using the needle valve in the ion gun.
11. Check the current again because pressure affect the current vie internal resistance. Make sure that you have selected the right layer on thickness monitor (see parameter table A.1)
12. Make sure that all parameter are right for the evaporation and then open the shutter (on the left side of the chamber). Reset the thickness to zero by pressing RUN once or twice (first must go to the closed mode and then return to the open mode)
13. Evaporate you layer. Keep evaporation parameter as constant as possible: pressure, rate and temperature should stay the same as in the calibrations.
14. When you have the target thickness in monitor, close the shutter rapidly and press run to set the thickness monitor to stop.
15. Turn the current knob to zero value and then turn the current off (red button).
16. Close the needle valve.
17. Let the crucible liner cool down for some minutes until it is no longer glowing (no visible red colour seen).
18. Evaporate next layer(s) using steps 2–17.
19. When all layers are evaporated, close the gas line (O_2) and close the needle valve (if not already closed).
20. Turn of the HIGH VOLTAGE and the MAIN POWER.
21. Let the GUN WATER flow at least half an hour after stopping the evaporation because it needs to cool down in a controlled way!

Table A.1: Available dielectric materials with their positions and proper evaporation conditions. Layer numbers are programmed to the thickness monitor. Positions are given counter clockwise starting from the empty slot. Tooling factors (TF) may vary from time to time and depend on pressure, p, and evaporation rate.

Layer number	Material	Crucible liner position	Typical TF	p, mbar	Evaporation rate, nm/s	Current, mA
1	Al_2O_3	1	1.40–1.55	$3.0{\cdot}10^{-5}$	0.1	60–90
2	SiO_2	2, 3	1.10–1.15	$3.0{\cdot}10^{-5}$	0.2–0.25	15–35
3	TiO_2	4	1.53–1.62	$1.2{\cdot}10^{-4}$	0.1–0.15	90–125
4	Ti_3O_5	5	1.7–1.85	$7.0{\cdot}10^{-5}$	0.1–0.15	90–110

22. Unload your samples: warm the chamber with hot water etc.

23. Pump down the chamber and leave all water lines closed.

Calibration of the thickness monitor

1. Load a piece of material that you can measure with an ellipsometer.

2. Proceed as if you were evaporating a single layer of material of your interest.

3. Evaporate e.g. 70.0 nm according to thickness monitor and then close the shutter.

4. Unload the calibration sample and pump down the chamber.

5. Measure the thickness and refractive index.

6. Set the Tooling Factor to a new value given by equation

$$TF = TF_{old}\frac{d_{measured}}{d_{set}},$$

where d_{set} is that 70.0 nm (=700Å) you evaporated, $d_{measured}$ is the actual thickness you measured with an ellipsometer and TF_{old} is the tooling factor you used during the evaporation.

7. Repeat the calibration for all the materials you will need.

Changing the thickness monitor crystal

Thickness monitor has a gold-coated crystal, which is modulated with 6 MHz frequency. This crystal works only for small amounts of material deposited on the crystal surface. If too much material is deposited, then the thin film is too thick for the monitor to calculate the grown thickness and the accuracy becomes poor. This is why the device has usage number. When the number is higher than 140, the crystal should be changed if a good accuracy is needed. The crystal should be changed no later than the number reaches 190; after that the crystal can just break and leaving the user totally blind for the growth rate.

1. Open the loading chamber.
2. Open the two small screws beside the crystal holder and pull the top cover carefully up.
3. Use tweezers to remove the used crystal.
4. Clean the hole for crystal from flakes.
5. Place a new crystal into the crystal holder; remember to place the crystal the three contact surfaces upwards.
6. Push the cover carefully back and make sure that it is all the way down. This might sometimes be difficult but it works when the cover is straight. Use of excess force is NOT needed.
7. Close the two screws and verify that usage in the monitor is less than 10. If there is no reading, there is probably a bad contact. In that case, check that the contacts are upward and try to put the cover better (steps 6–7). Remember to ask help if problems occur.

Periodic maintenance work

To operate the device normally it does not need any special procedures. However, to sustain this status electron beam evaporator needs to maintenance once in a while. In the following there is listed the routine maintenance work with suggestion for how often they should be performed.

1. Clean the gun chamber with vacuum cleaner. The bottom is reached through the maintenance hatch on the opposite side to turbo pump. It can be opened with a wrench; when you close it, remember that it is important to close it homogenously, so first close all nuts lightly and then all of them with a bit more force. The gun should be cleaned from the top so that no waste material drops or flakes are left on the copper surface. Usually after this also new materials are added. Full cleaning of the chamber should be performed almost every month.

2. Adding material can be done through the hatch in front of the device. If some crucible liners are damaged, ask help from more experienced users and do not lift them away by yourself. Add materials to the crucible liner (= cup where the material is, crucible is the copper excavation, which is water cooled) with a special, clean spoon. The spoon is in a plastic cover and should be located in the same box as all the evaporation materials (on the right). You can also use clean tweezers for bigger tablets (e.g. TiO_2 is often as 5 mm diameter grains). When you load materials you should be absolutely sure that you add the right material and that you know how to do it. After adding material to a crucible liner, material has to be melted and the calibration takes a lot of time. This is why you should have some kind of idea, when adding is really needed and when you can proceed normally. Usually new materials are needed 1–3 times a month in research use depending on the amount of evaporated films.

3. Change of e-beam filament is a very rare operation and should not be done without the person in charged of the device. Further instructions are given in the operation manual.

4. Changing the thickness monitor crystal is a normal procedure and it is needed when the usage is too high (>140). If high accuracy is not needed in the following evapor-

ations, then you can use the crystal till the usage is 190. Crystal needs to be changed typically 2–4 times a month.

5. In the control rack there are orange lights indicating the status of the valves and pumps: sometimes those lamps burn. Changing the lamp is quite straight forward: pump down both chambers and make sure that you are in AUTO-mode, then turn the control to OFF-mode, remove the orange cover, pull the lamp away (tip: a plastic hose of proper diameter can help in this a lot) and push the replacement in the hole. WARNING: make sure that the chambers are pumped down because this work can easily cause short circuits in the control automation. In such event an open loading camber and closed gun chamber could have catastrophic results for the turbo pump. After replacing the lamp(s) return to AUTO-mode.

6. When the controls are in MANUAL-mode all buttons try to fulfill their purpose immediately. Therefore, do not use manual mode unless you know what you are doing. This might damage the vacuum system. Manual mode is used in cases when automatic controls are not working properly or they are jammed (can happen if automatic processes are interrupted in a wrong state. Remember that a light on means that the valve is open and a light off means that is closed. Do not push different buttons too fast or simultaneously because it takes some time for the valves to close; especially the main valve between gun and loading chamber has a slow operation speed. You can verify the main valve state from the upper side of the valve servo: there is a text open and closed and there is white arrow pointing to the current state.